MNRAS 000, 1–19 (2022) Preprint 10 November 2022 Compiled using MNRAS LATEX style file v3.0

Time series analysis of bright *TESS* RRc stars: Additional modes, phase variations and more

J. M. Benkő,[1,2]★ E. Plachy,[1,2,3] H. Netzel,[1,2,4] A. Bódi,[1,2,3] L. Molnár[1,2,3] and A. Pál[1]
[1]*Konkoly Observatory, Research Centre for Astronomy and Earth Sciences, ELKH, MTA Centre of Excellence, Konkoly Thege Miklós út 15-17, H-1121 Budapest, Hungary*
[2]*MTA CSFK Lendület Near-Field Cosmology Group*
[3]*ELTE Eötvös Loránd University, Institute of Physics, Pázmány Péter sétány 1/A, H-1117 Budapest, Hungary*
[4]*Nicolaus Copernicus Astronomical Centre, Polish Academy of Sciences, Bartycka 18, PL-00-716 Warsaw, Poland*

Accepted XXX. Received YYY; in original form ZZZ

ABSTRACT

Using two years of data from the *TESS* space telescope, we have investigated the time series of 633 overtone pulsating field RR Lyrae (RRc) stars. The majority of stars (82.8 per cent) contain additional frequencies beyond the main pulsation. In addition to the frequencies previously explained by the $\ell = 8$ and $\ell = 9$ non-radial modes, we have identified a group of stars where the additional frequencies may belong to the $\ell = 10$ non-radial modes. We found that stars with no additional frequencies are more common among stars with shorter periods, while stars with longer periods almost always show additional frequencies. The incidence rate and this period distribution both agree well with the predictions of recent theoretical models. The amplitude and phase of additional frequencies are varying in time. However, no clear relationship was found between the period of these variations and the period of the main pulsation. The time dependence of the different frequencies seems to be different. We also found signs of time dependence for the f_{68} frequencies. We have determined a 10.4 per cent incidence rate for the Blazhko effect. For several stars we have detected continuous annual-scale phase change without significant amplitude variation. This type of variation offers a plausible explanation for the 'phase jump' phenomenon reported in many RRc stars. The main pulsation frequency could show quasi-periodic phase and amplitude fluctuations. This fluctuation is clearly related to additional frequencies present in the star. The summation of this phase fluctuation over time may explain the O−C variations that have long been known for many non-Blazhko RRc stars.

Key words: stars: oscillations – stars: variables: RR Lyrae – asteroseismology – techniques: photometric – methods: data analysis – space vehicles

1 INTRODUCTION

The almost continuous observations of current photometrc space telescopes allow us to study moderate to small-amplitude brightness variations in stars. In the last decade and a half, thanks to these space missions, we have discovered many interesting phenomena, even in classical radially pulsating variable stars, such as the Cepheid or RR Lyrae stars. One of these is the appearance of low-amplitude extra modes in pulsating variables in the first radial overtone.

To the best of our knowledge, the first observation of such additional frequencies was made with the small Canadian space telescope, *MOST*, in the RRd star (which pulsates in the fundamental and first radial modes simultaneously) AQ Leo (Gruberbauer et al. 2007). Shortly afterwards, Olech & Moskalik (2009) found two overtone-pulsating (RRc) stars in the ground-based measurements of the globular cluster ω Cen whose Fourier spectra revealed f_x extra frequencies such that the ratio to the f_1 dominant frequency is $f_1/f_x \approx 0.61$. In four RRc stars known at that time in the field-of-view of the *Kepler* space telescope, Moskalik (2013); Moskalik et al. (2015) presented a complex additional frequency structure, and the ratios of the highest amplitude additional frequencies also fell between 0.612 and 0.632. All RRc and RRd stars observed by *CoRoT* satellite also contain these extra frequencies (Chadid 2012; Szabó et al. 2014). In parallel with the studies on RR Lyrae stars, similar additional modes have also been found in overtone Cepheids in the OGLE survey (Moskalik & Kołaczkowski 2009; Soszyński et al. 2008, 2010). In the case of Cepheids, three groups of stars could be identified from the larger sample, giving ratios of 0.61, 0.63 and 0.64, respectively. These stars are located on parallel sequences in the Petersen diagram. Based on the large OGLE database, Netzel et al. (2015a) and Netzel & Smolec (2019) showed that RRc stars showing extra modes also lie in parallel sequences on the Petersen diagram, similarly to the Cepheids. These sequences are at 0.613, 0.622 and 0.631 period ratios.

The current theoretical explanation of these extra frequencies is that they are associated with non-radial p-modes (Dziembowski 2016). The ratios $f_1/f_x \approx 0.61$, 0.63 and 0.64 belong to $\ell = 9, 8$ and 7 modes, respectively. A peculiarity of this explanation is that the observed signals at these ratios are the first harmonics of the true pulsation frequencies. The sequence at 0.622 of the overtone

★ E-mail: benko.jozsef@csfk.org

RR Lyrae stars is explained by linear combination frequencies that appear in the spectra.

Netzel et al. (2015a) pointed out that some of the RRc stars also show extra frequencies around the period ratio of 1.458. These frequencies are lower than the fundamental mode frequency of the star. For presentation reasons the inverse ratio ($f_x/f_1 \approx 0.686$) is used generally. For these frequencies, no theoretical explanation has yet been found.

The incidence rate of the the additional modes in RRc stars is rather controversial. The work that used the largest ground-based observational sample (OGLE survey, Netzel & Smolec 2019) obtained 9.6 per cent for the incidence rate in the Galactic bulge, while the space photometric rates, obtained for much smaller sample of field RRc stars, are between 81 and 100 per cent (Szabó et al. 2014; Moskalik et al. 2015; Molnár et al. 2015, 2022; Kurtz et al. 2016; Sódor et al. 2017; Forró et al. 2022)

The analysis of space photometric data is not limited to providing a better understanding of the additional modes. Continuous space data series can also answer some long-standing questions such as what causes the strong and often irregular period (O-C) variations observed in many RRc stars, which cannot be explained by stellar evolution (see Jurcsik et al. 2001, 2015 and further references therein). Or, how the so-called 'phase jump' phenomenon happens: the light curves of some RRc obtained in different observing seasons could not be folded by a common period. However, if we assume that there was a phase jump between the observing seasons, the light curves can be folded nicely (e.g. Wils et al. 2007; Wils 2008). Is this a real, sudden jump or the result of a continuous phase change during the non-observed time interval? The work of Moskalik et al. (2015) on *Kepler* RRc stars suggests the second scenario, but their sample of four stars is too small for a final answer. Only continuous observation on a larger sample can decide the question.

The observations of the near all-sky *TESS* mission gives us a good opportunity to investigate RRc stars through a large and homogeneous sample of space photometry.

2 DATA AND DATA PROCESSING

In this paper, we used measurements from the *TESS* (Transiting Exoplanet Survey Satellite) photometric space telescope. The detailed specification of the satellite can be found in Ricker et al. (2015). Here we just briefly summarize the most important facts.

NASA has launched *TESS* in spring 2018. It uses its four wide-angle CCD cameras to scan 24° of the sky, one 96° × 24° area at a time, known as sectors. *TESS* orbits the Earth in a high and highly elongated orbit (with a perigee of 108 000 km and an apogee of 375 000 km, i.e. an orbital eccentricity of 0.55), the orbital period is 13.7 d. One sector is observed in two orbits. In its first year of operation, the space telescope surveyed 13 sectors of the southern (ecliptic) sky, and in its second year it continued its work in the northern sky. This work uses data from the first two complete years of observations, i.e. 26 sectors. Since sectors have overlapping areas many of our targets have data from multiple sectors, some of which are located in the continuous viewing zones near the ecliptic poles that were observed for nearly over a year.

The integrated exposure time of the cameras was 30 minutes for the first two years. The resulting so-called full frame images (FFIs) were used.

2.1 The sample

Our primary goal is to detect and analyse the frequency content of RRc stars on a large homogeneous space photometric sample. Our sample is based on the catalog of Clementini et al. (2019), which lists more than 40 380 RRc stars across the sky observed by *Gaia* space mission. Since the additional modes are usually associated with low amplitude frequencies, we restrict ourselves to using the best quality data series. The quality of the *TESS* time series depends primarily on the brightness of the star and the crowding. Therefore, brighter than G_R =14 magnitude RRc stars measured by *TESS* were selected for our sample. (Note that the throughput function of *TESS* cameras is close to the function of this G_R broadband filter of *Gaia*, therefore, we use it in this paper as a representation of apparent brightness.) The brightness of the brightest observed RRc star (CS Eri, G_R = 8.672 mag) is well bellow the saturation limit of *TESS* photometry (~ 7.5 mag, Ricker et al. 2015). This brightness limit seemed a good compromise: the resulting sample is large enough (747 stars), since above 14 magnitude the noise starts to increase rapidly (Lund et al. 2021).

Beside the observational noise there is another effect that can cause significant degradation in the data quality, the scattered light from the Earth and the Moon. The correction of this effect often needs much more effort than a simple detrending, therefore we excluded stars with strong systematics, and focused on the best quality light curves. This selection resulted in a sample of 666 elements. We added additional four bright RRc stars which are missing in the list of Clementini et al. (2019) but observed by *TESS*. The final 670 stars of our sample are listed in (the electronic version of) Table 1 sorted by right ascension. The table shows the traditional name (if it exists, col. 1) position from the *Gaia* DR2 data base (cols. 2-3), the apparent brightness in the *Gaia* G_R-band (col. 4) and for convenience, we include the *TESS* TIC IDs (Stassun et al. 2019) in the last column. Since many stars were observed more than one sectors, in total, 1357 time series were analysed.

The distribution of our sample in the sky is illustrated in Fig. 12. Stars are missing in areas where *TESS* has not measured in its first two seasons: along the plane of the ecliptic and a part of the northern ecliptic hemisphere (where scattered light from the Earth or Moon made observation impossible).

2.2 Data processing

To produce FFI light curves we used the differential-image pipeline developed by Pál (2012) in which the key element is an image convolution step that is able to correct for many of the instrumentation effects. This tool has already been applied to *TESS* RR Lyrae stars in the study of Molnár et al. (2022). For a more detailed description of the pipeline we refer to Plachy et al. (2021), where it was used on Cepheid stars. Since our analysis is sensitive to contamination from neighboring stars, we chose a relatively small circular aperture with 1.5 pixel radius even if this led us to an underestimation of the amplitude of the brightness variation. We derived the flux zero-point with respect to the *Gaia* G_R magnitudes (Gaia Collaboration et al. 2018). For further corrections we applied a detrending algorithm based on polynomial fitting that was optimized by phase dispersion minimization (Bódi et al. 2022) and removed outliers with a sigma-clipping process. For most of the stars we have data from multiple sectors: these light curves were stitched together, with brightness differences between sectors corrected by scaling and shifting.

Table 1. Basic parameters of the used *TESS* RRc sample

Star	RA deg	DEC deg	G_R mag	TIC ID
Gaia DR2 2880528638650410624	0.1847089694	37.8428564459	12.73282	432552294
AO Tuc	1.0265057115	−59.4852399803	10.849399	201252114
2MASS J00120716-5523075	3.0299739036	−55.3854498465	13.675732	201292299
V1035 Cas	6.9957719417	49.1625628476	11.720211	202550541
CO Tuc	7.141191811	−72.16913968	13.628787	267215550
...				

The full-size table is available in machine-readable format in the electronic supplement.

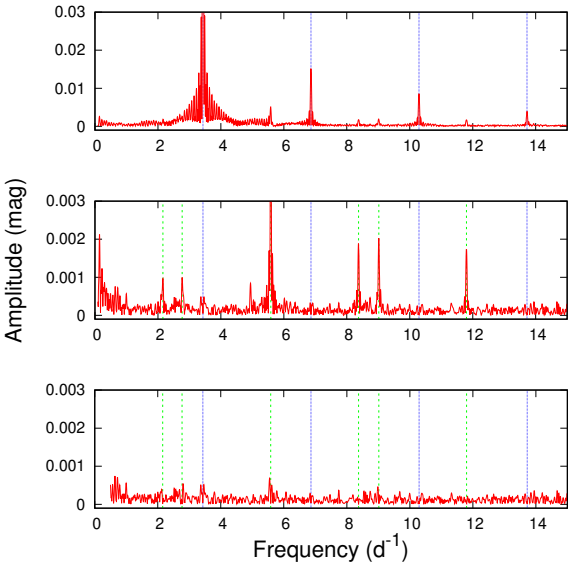

Figure 1. Main steps of the Fourier analysis. The Fourier spectrum of the observation of GV Her in Sector 24 (top). The blue dotted vertical lines show the location of the main pulsation frequency and its harmonics. In the middle is the pre-whitened spectrum and the significant additional frequencies found therein (indicated by green dashed lines). The residual spectrum (bottom) is pre-whitened with all frequencies indicated. Note the different amplitude scales.

3 FOURIER ANALYSIS OF THE LIGHT CURVES

3.1 The process and its results

For Fourier analysis of space photometric data of RR Lyrae stars there are numerous suitable software packages. Whichever has been tested for this purpose they all give the same results for frequencies, amplitudes and phases within error (Chadid et al. 2010; Benkő et al. 2010). Due to its simple automation, the SigSpec package (Reegen 2007, 2011) was chosen for the present analysis. We ran SigSpec twice for each data set. First, we determined the dominant pulsation frequency f_1 by fitting three-five of its harmonics (see Table 2), then we pre-whitened the data series with the dominant frequency and these harmonics, and searched consecutively for all significant frequencies ($S_f > 5$) in the residual, where S_f means the spectral significance defined in Reegen (2007). In the first run, the frequency search was performed between 0 and the Nyquist frequency (24 d^{-1}). In the second run, both the low- and high-frequency parts were truncated for faster running, so that additional frequencies were searched between 0.5 and 15 d^{-1}. Fig. 1 illustrates the process with one of GV Her data set while numerical results are shown in Table 2 and Table 3.

Table 2 contains the name of the stars (col. 1), the number of used sectors (col. 2), the dominant pulsation frequency (col. 3) and its Fourier amplitude (A_1, col. 4). The Fourier parameters in cols. 5-8 are defined the usual way: $R_{21} = A_2/A_1$, $R_{31} = A_3/A_1$, $\phi_{21} = \phi_2 - 2\phi_1$ and $\phi_{31} = \phi_3 - 3\phi_1$ (Simon & Lee 1981). Here the amplitudes and phase (A_i, ϕ_i, $i = 1, 2, 3$) are derived from sinus-based Fourier solutions as

$$m(t - t_0) = m_0 + \sum_{i=1}^{N} A_i \sin\left[2\pi i f_1 (t - t_0) + \phi_i\right], \quad (1)$$

where $m(t)$ is the light curve, m_0 the zero point (the average brightness), $N = 3, 4$ or 5. The starting epoch t_0 is always the observed time of the first element of the given data sector. In the case where a star was detected in more than one sector, the frequencies, amplitudes and Fourier parameters are calculated from the merged data sets. Last column contains some remarks. The underlying meaning of these notations is explained in Sec.4.1 and Sec.4.2.

The Table 3 shows the result of the Fourier analysis on the residual light curves after we subtracted a non-linear fit containing the main frequency and its harmonics. The consecutive pre-whitening and frequency search was carried out on each data set separately. The name of the data sets (col. 1), consisting of the name of the star and the number of the *TESS* sector. Next columns show the dominant frequency f_1 (col. 2) its Fourier amplitude and phase (A_1, ϕ_1 in cols. 3-4). The additional columns list the frequencies (col. 5), amplitudes (col. 6) and phases (col. 7) associated with the extra peaks according to the pre-whitening steps, with decreasing amplitudes. Columns 8 and 9 give the period and amplitude ratios of the given frequency and the main frequency, respectively. The last column shows the possible identification of the frequency (see later).

The numerical values in Table 2 and 3 give the significant decimal digits plus one additional digit. The frequency accuracy can be estimated by the Rayleigh frequency resolution value. In our case, it is between 0.037 and 0.0027 d^{-1}, depending on the length of the data series. Practical experience and e.g the work of Kallinger et al. (2008) show that the Rayleigh resolution strongly overestimates the error of the frequencies. If we calculate the average frequencies and their standard deviation of stars measured in more than one sector, we obtain for $\sigma(f_1)$ between $1.0 \cdot 10^{-6}$ and $5 \cdot 10^{-4}$ d^{-1}. That is, the frequency can be determined to an accuracy of about four digits. We assume that this is also true for the frequency of stars measured in only one sector. Accordingly, the frequency is given to 5 decimal digits in Table 2. For the other Fourier parameters we proceed in a similar way.

3.2 Fourier parameters vs. period planes

In Fig. 2 we plot the R_{21}, R_{31}, ϕ_{21} and ϕ_{31} Fourier parameters given in Table 2 as a function of the dominant period ($P_1 = 1/f_1$).

Table 2. Results of the Fourier analysis

Star	Sec.	f_1 d^{-1}	A_1 mag	R_{21}	R_{31}	ϕ_{21} rad	ϕ_{31} rad	Remark
2MASS J00120716-5523075	3	3.19373	0.0971	0.216	0.052	3.042	−0.394	Bl,f_{68},f_{61},blend?
2MASS J02253626-5519227	2	2.58304	0.1037	0.091	0.071	3.798	1.025	f_{68},f_{61},f_{63}
2MASS J03132028-1726447	1	3.80346	0.0974	0.166	0.036	3.035	−0.267	-
2MASS J03354606-2902102	1	3.60580	0.0999	0.215	0.067	3.025	−0.487	f_{61}
2MASS J04274606-6202513	12	3.39956	0.1161	0.199	0.050	3.014	−0.439	-
...								

The full-size table is available in machine-readable format in the electronic supplement.

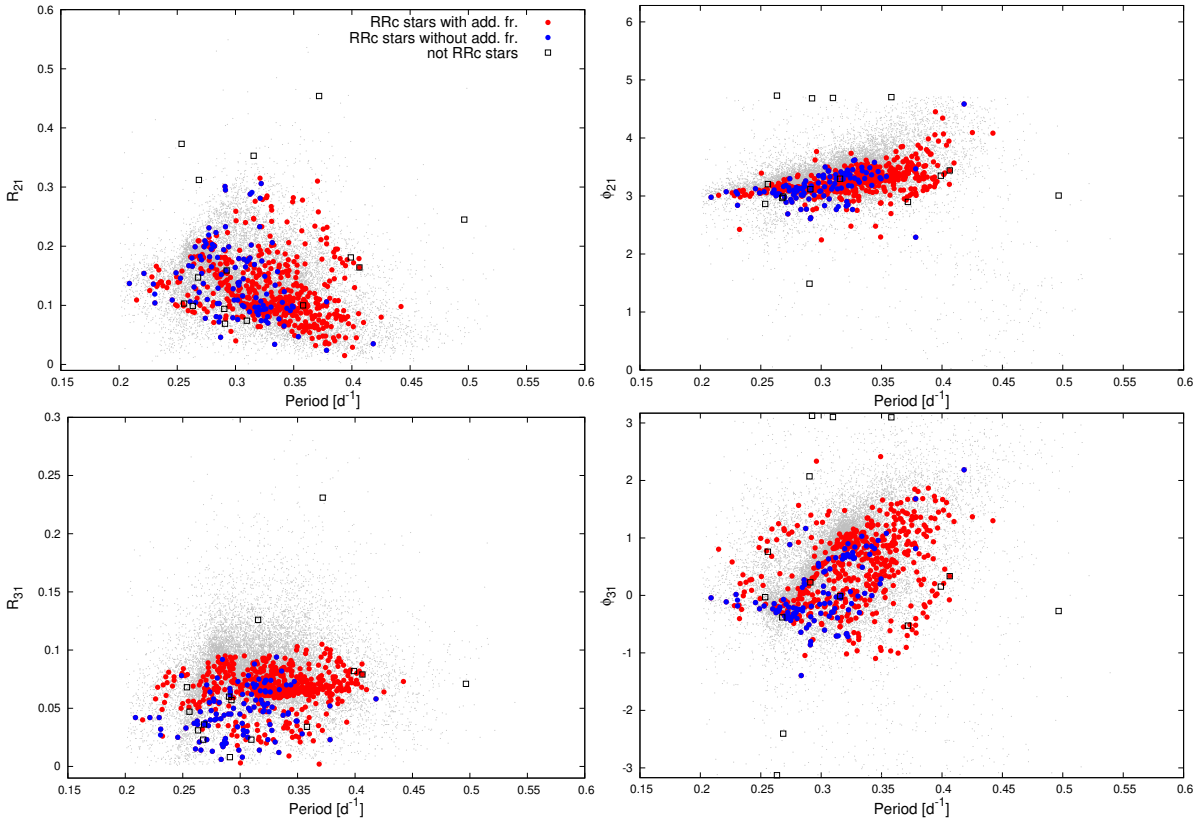

Figure 2. Fourier parameters R_{21}, R_{31}, ϕ_{21} and ϕ_{31} as a function of the pulsation period P_1. The red and blue symbols indicate stars that do and do not show additional frequencies, respectively. The empty black rectangles show the identified non-RRc stars listed in Table 4. For comparison, OGLE RRc stars are also shown (gray dots).

Table 3. Additional frequencies in *TESS* RRc Fourier spectra

Data set	f_1 d^{-1}	A_1 mag	ϕ_1 rad	f_x d^{-1}	A_x mag	ϕ_x rad	f_1/f_x	A_x/A_1	ident.
2MASS_J00120716-5523075_s1	3.19360	0.0963	−0.0420	3.09213	0.0190	0.6752	0.968	0.198	$f_1 - f_B$
2MASS_J00120716-5523075_s1	...	...	...	3.30145	0.0033	2.7865	0.967	0.035	$f_1 + f_B$
2MASS_J00120716-5523075_s1	...	...	...	2.16806	0.0032	1.8787	0.679	0.034	f_{68}
...									
2MASS_J00120716-5523075_s2	3.19385	0.1066	1.3243	3.09200	0.0214	1.1599	0.968	0.201	$f_1 - f_B$
2MASS_J00120716-5523075_s2	...	...	...	2.17098	0.0037	−1.8961	0.680	0.035	f_{68}
2MASS_J00120716-5523075_s2	...	...	...	6.28551	0.0036	2.8806	0.508	0.034	$2f_1 - f_B$
...									

The full-size table is available in machine-readable format in the electronic supplement.

Table 4. List of identified non-RRc stars

Gaia DR2 ID	RA deg	DEC deg	G_R mag	Star	Note
5073663940716363904	46.7627438301	−26.0423842601	9.703495	HD 19479	W UMa
3295420894600845952	75.0391559681	12.7591150306	13.9129		RRab
5256789350372915328	149.687401418	−59.4632677075	12.035355		RRd
5202509386185816704	149.902329174	−78.7385930078	13.073698		Ecl?
1066922279223207040	152.8130218992	67.6083869718	13.832476		HADS?
5234537300921901824	171.255477458	−69.2574940474	12.416878		RRab
3513784423567794688	186.2895988837	−21.6645591793	11.9342	XX Crv	RRd
067166601592685440	201.7892016557	−53.9859257004	13.659541	BT Cen	RRab
1588420094522305024	229.3719083681	48.1918167858	13.550349	CRTS J151729.2+481131	RRd
1342291874024443008	264.657398107	37.0837733568	13.847074	CRTS J173837.7+370502	W UMa
2092889154772199168	284.9514704246	36.1800009151	12.624741		W UMa
2089300658056315776	302.1361662576	52.9588098225	12.884088		W UMa
2005340708908381696	331.6717909237	53.8447046694	13.663897		W UMa
1956531880221332480	332.5323465599	40.9195805444	9.764321	DE Lac	HADS?

It can be clearly seen that the vast majority of stars lying a well-defined area in each panel of the figure. These areas overlap strongly with the areas defined by the OGLE sample (Soszyński et al. 2014, 2016a, 2019), but some significant shifts can also be found between them. As already noted by Molnár et al. (2022) the sensitivity function of the *TESS* cameras and the *I*-band filter used by the OGLE team are close but not identical. They found that the R parameters are nearly identical, but there is a phase shift in the ϕ parameters. From our much larger element sample, however, a small amount of shift (≈ 0.015) is also seen for the R_{31} parameter.

The stars that are located far from the main areas have been examined one by one to identify what causes their deviant position. A common reason is that two nearby stars are blended by *TESS*. Such stars were verified by examining their unusual light curves, Fourier spectra and raw CCD images. For the 22 such identified stars, the word 'blend' is added to the note column of Table 2. These stars are not plotted in Fig. 2 and their frequencies are also not listed in Table 3. For a further 28 stars, only one of the measured sectors was blended or the fact of blending was not sure. These stars were marked as 'blend?' in Table 2 and their data were used for the analysis. We note that the Fourier parameters of these stars are not significantly different from those of the un-blended stars.

Unlike those that turned out not to be RRc stars. This was the second most common reason for the unusual Fourier parameters. The 14 identified non RRc stars are collected in Table 4 where we also give their possible classification. Their position are shown by empty rectangles in Fig. 2. Omitting the non RRc stars and those that were certainly blended, we got a 633 element sample for further analysis.

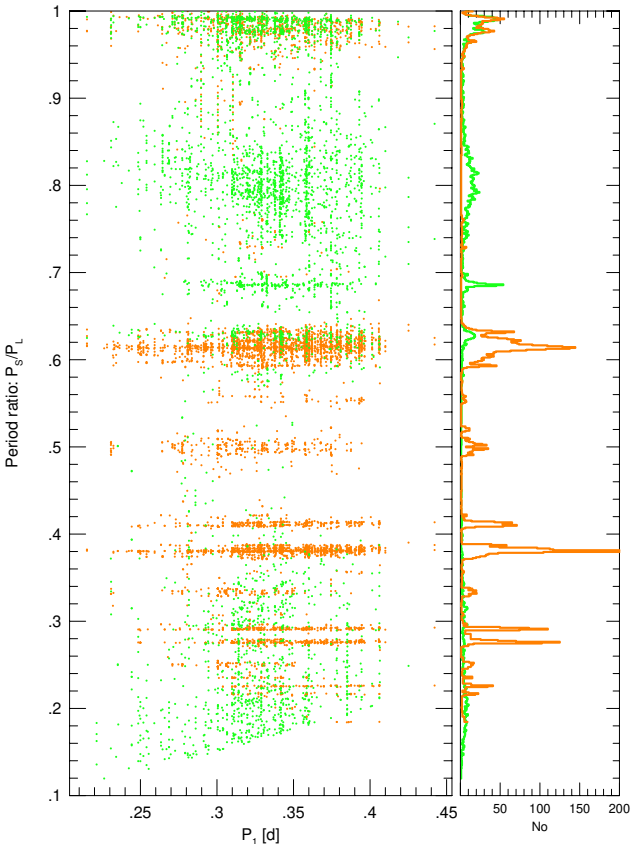

Figure 3. Left panel: period ratio between additional mode P_x and dominant pulsation period P_1 in the function of P_1. According to the former studies, the smaller period P_S is divided by the larger one P_L, so the values of period ratio are between 0 and 1. Orange symbols: $P_x/P_1 < 1$, green symbols: $P_x/P_1 > 1$. Right panel: histograms show the additional frequency incidence rates as a function of the period ratio.

4 ANALYSIS OF THE SAMPLE

Beyond the main pulsation frequency (and its harmonics) we detected more than 11 000 significant frequencies on the 633 analysed stars.

All the detected frequencies are plotted in a Petersen like diagram in Fig. 3. Each point of the figure belong to a frequency of a certain observed sector of a given star. That is, the frequency content of each sector of each star is included here. We show this because the amplitude of frequencies could depend on time and therefore the frequency content of different sectors might be different. Following the former studies the period ratio are calculated as P_S/P_L, where P_S and P_L the smaller and the larger periods, respectively. This representation results a compact diagram but it also has disadvantages. In the figure, orange symbols indicate $P_x/P_1 < 1$, while green symbols indicate $P_x/P_1 > 1$. It can be seen that with large number of frequencies, the ratios of the distant frequencies could close to each other, mixing and making the interpretation difficult.

The detected frequencies are not randomly distributed in Fig. 3, but grouped at certain period ratios. A histogram of the frequency distribution was constructed by dividing both intervals ($P_1 > P_x$ and $P_1 < P_x$) into 0.001-wide bins and plotting the number of frequencies in each bin in the right panel of Fig. 3. In the unstructured part of the figure, each bin of the histogram contains 1-3 frequencies. The significant deviation from this random distribution was chosen to be three times of this value (9 frequencies per bin). Although this choice is somewhat arbitrary, it is a good representation of what we see when we look at the figure.

The frequencies were first identified automatically by assuming that the spectra of stars can contain similar frequencies as seen for *Kepler* stars (Moskalik et al. 2015; Sódor et al. 2017). Namely, (i) Blazhko side-peaks ($f_1 \pm f_B$, $2f_1 \pm f_B$, etc.), (ii) frequencies of probable non-radial modes, various harmonics and sub-harmonics of them (f_{61}, f_{63}, $0.5f_{61}$, $1.5f_{61}$, ...), (iii) and linear combinations of these frequencies to each other and with the main pulsation frequency.

The automatic frequency identifier works by taking all the frequency combinations in the *Kepler* RRc stars in the work of Moskalik et al. (2015) and calculating their possible values for a given star. We then form the difference between the actual to be identified and the calculated frequencies. The differences are sorted and if the smallest difference is less than 0.05 then we accept that the observed frequency is the same as the hypothesized combination. The automatic identification was manually checked one by one and was modified if it was incorrect. The result of this process is given in column 10 of Table 3 as a possible identification. The imperfectly removed long-term instrumental trends also appear as side peaks, similar to the long-period Blazhko effect. In such cases, the word 'long' is included in this column. A side result of the manual check is that few additional non-RRc stars are filtered out. These are also included in Table 4 (and already excluded in the final 633-element sample).

4.1 The Blazhko effect

Stars showing the Blazhko effect (i.e. correlated amplitude and frequency modulation of the main pulsation) are usually searched for in larger databases by detecting side peaks in the Fourier spectra next to the main frequency and harmonics. If we searched our sample using this criterion, we found side peaks for 250 stars. These frequencies are located in the dense regions around $P_S/P_L \sim 1.0, 0.5, 0.33, 0.25$ in Fig. 3. These ratios correspond to the ratios of the side peaks to the main frequency: $f_1/(f_1 \pm f_B)$, $f_1/(2f_1 \pm f_B)$, $f_1/(3f_1 \pm f_B)$ and $f_1/(4f_1 \pm f_B)$, respectively.

On closer inspection of the light curves and Fourier spectra of the stars showing the above frequencies can be divided into two main groups: (i) In one group the light curves show a clear variation in amplitude, and – more importantly – if there have been observations of the star in several sectors, all their spectra show the same side peak frequencies. The side peaks generally form a regular multiplet structure (triplet, quintuplet, etc) although sometimes side peaks on one side are significant only. (ii) In the other group there is no visible amplitude variation, and the distance of the side peaks from the main frequency varies from sector to sector, and what is more, in some sectors there are no significant side peaks at all. It is also common to show not regular multiplets but complex forest of peaks.

The first group shares all the characteristics of stars with the 'classical' Blazhko effect. In total, 68 such RRc stars were found in our sample, representing 10.7 per cent of all stars. These stars are marked with a sign 'Bl' in the last column of Table 2. The work of Netzel et al. (2018) has recently reviewed the incidence rate of the Blazhko effect for different groups of stars (see Table 4 in their paper). The value for the Galactic field RRc stars is not included in the table, as no study has yet been done that has analysed a larger number of field RRc stars in a homogeneous way. The missing value can now be added to the table: our rate of 10.7 per cent here is in good agreement with the 13 per cent value of Molnár et al. (2022) who used data from the first two sectors of *TESS*, only.

The previously obtained values fell between 4 per cent (for the LMC) and 19 per cent (for the NGC 6362). As opposed to SMC and LMC, in the case of stars in the Galaxy, all previous studies have shown that the Blazhko effect is 3–5 times more frequent in RRab stars than in RRc stars. This remains true even if only space photometric measurements are taken into account. The incidence rate of Blazhko RRab stars in the much smaller *Kepler* sample is 51–55 per cent (Benkő et al. 2019), while Molnár et al. (2022) obtained a ratio of 47.5–70.7 per cent for a subset of *TESS* RRab stars (82 stars), Plachy et al. (2019) found the 44.7 per cent of 371 K2 RRab to be Blazhko stars, but Kovács (2018) even found 91 per cent of 151 K2 RRab stars to be modulated.

What about the second group? As mentioned in the introduction, RRc stars often contain non-radial modes (a detailed discussion of these is given in next section). The amplitude and value of the frequencies associated with these modes is known to vary in time, and as Moskalik et al. (2015) has shown, the main periods vary anti-correlatedly with this variation. The quasi-periodic nature of this variation explains the forest of side-peaks and the appearance of different 'modulation' frequencies from sector to sector. In short, in this case there is no Blazhko effect, but we see a reflection of the time variations of the non-radial modes in the Fourier spectra. The phenomenon is investigated in Sec. 5.

4.2 Additional frequencies

In this section, we refer to all significant frequencies that are not belong to the main pulsation or the above discussed phenomena (the Blazhko effect and low amplitude quasi-periodic modulations) as additional frequencies. If we omit the identified Blazhko frequencies and frequencies belonging to longer than 10 days period variations (e.g. instrumental trends, satellite orbit), 524 stars (82.8 per cent of the complete RRc sample) remain, where we found frequencies corresponding to a signal with a significant frequency. It is emphasized that we were not looking for frequencies with a given frequency ratio, but for all significant frequencies in the interval between 0.5 and 15 d^{-1}.

The incidence rate of the additional mode frequencies of the previous works are quite different from each other. The combined incidence rate (including the f_{61}, f_{63} and f_{68} groups) has been found to be 27 and 63 per cents in high-cadence OGLE fields and in the globular cluster NGC 6362, respectively (Netzel et al. 2015b; Smolec et al. 2017). Jurcsik et al. (2015) obtained for f_{61} stars a 38 per cent rate in the M3 globular cluster. For frequencies with a periodic ratio between 0.60 and 0.64, the incidence rate of the Galactic bulge was 8.3 per cent from the OGLE data, while for frequencies with a periodic ratio $\sim$ 0.68, it was 1.3 per cent (Netzel & Smolec 2019).

Additional mode frequencies have been detected in all previously published (small number of) overtone RR Lyrae stars measured by space photometry with *CoRoT* and *Kepler* (Szabó et al. 2014; Moskalik et al. 2015; Molnár et al. 2015; Kurtz et al. 2016; Sódor et al. 2017). Each of the small, 4-element sub-sample of K2 also shows additional frequencies (Molnár et al. 2015). By using 31 selected stars measured in the first two observing sectors of *TESS* satellite, Molnár et al. (2022) determined the incidence rate of RRc stars with addi-

Table 5. Positions and probable identifications of the horizontal ridges in Fig. 3

Ratio P_x/P_1 (P_1/P_x)	Size ×0.001	No.	Ident.
0.216	3	56	$3f_1 + f_{61,62,63}$
0.226	3	94	$2f_1 + 1.5f_{61}$
0.235	1	30	$f_1 + 2f_{61}$
0.272	1	20	$2f_1 + f_{60}$; $3f_1 + f_{68}$
0.275	6	377	$2f_1 + f_{60,61,62,63}$
0.291	5	329	$f_1 + 1.5f_{61}$; $f_1 + f_{61} + 0.5f_{63}$
0.297	2	22	$f_1 + 1.5f_{63}$
0.372	4	42	$2f_1 + f_{68}$
0.376	5	125	$f_1 + f_{60}$
0.380	7	662	$f_1 + f_{61}$
0.383	3	312	$f_1 + f_{62}$
0.387	5	146	$f_1 + f_{63}$
0.410	3	217	$1.5f_{61}$
0.412	4	153	$f_{61} + 0.5f_{63}$
0.417	2	27	$1.5f_{63}$; $f_1 + 2f_{68}$
0.552	3	26	$f_1 + 0.5f_{61}$
0.557	3	19	$f_1 + 0.5f_{63}$
0.593	10	149	$f_1 + f_{68}$
0.602	20	311	f_{60}
0.613	18	990	f_{61}
0.622	9	534	f_{62}
0.631	12	341	f_{63}
0.729	3	17	$2f_{68}$
1.197 (0.835)	33	208	$0.5f_{60}$
1.229 (0.814)	54	329	$0.5f_{61}$
1.264 (0.791)	30	420	$0.5f_{63}$
1.459 (0.685)	10	321	f_{68}
1.594 (0.626)	37	226	$f_{61} - f_1$

tional modes to be 81 per cent. The latter value is in good agreement with the 82.8 per cent we obtained. That is, it seems that additional frequency mode is present in most RRc stars, but not all. This is exactly the situation that Netzel & Smolec (2022) obtained from their theoretical models.

The lower incidence rates of ground-based surveys can be explained by the interaction of several causes. The fact that different detection limits are associated with different brightness of samples measured with detectors of different sensitivities, and that the difference in data series length and sampling due to the varying amplitudes of the additional frequencies is also not negligible.

4.2.1 *Frequencies connected with f_{61} and f_{63}*

In Table 5 we listed the most frequent period ratios viz. the visible horizontal ridges in Fig. 3. The columns of the table show the period ratios P_x/P_1 and P_1/P_x in brackets where $P_x > P_1$ (col. 1), the size (thickness) (col. 2), the number of points counted (col. 3), and the identification of the frequencies of the ridge (col. 4).

The most populated horizontal group of frequencies is at the period ratio of $P_x/P_1 = 0.613$ (denoted by f_{61} in Table 3 and 5). We detected this frequency on 360 stars (57 per cent of the sample). As mentioned in the introduction, this additional frequency was the first identified in the Fourier spectrum of stars pulsating in their radial overtone mode. According to the theoretical model of (Dziembowski 2016), this frequency is caused by an $\ell = 9$ non-radial mode. To be precise, this frequency is the harmonic of the actual mode frequency. That is, the actual mode is associated with the frequency of $0.5f_{61}$.

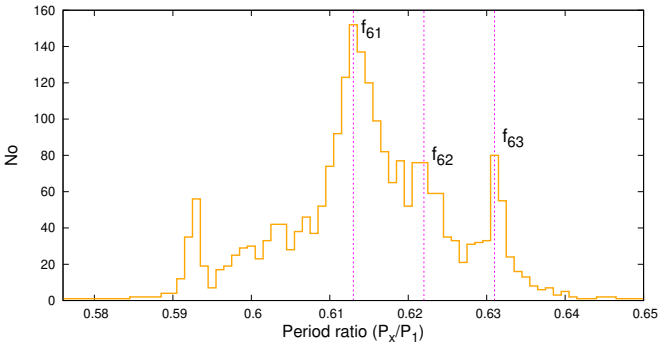

Figure 4. Distribution of the frequencies around the period ratio $P_x/P_1 = 0.61$. The dashed vertical lines show the positions the three ridges found in OGLE bulge data (Netzel & Smolec 2019).

This frequency was also observed on 186 stars. In many cases both f_{61} and $0.5f_{61}$ are significant, sometimes only one of them. The only reason for this phenomenon is that we look at stars from different angle of views, as shown by the work of Netzel & Kolenberg (2021). The third harmonic ($1.5f_{61}$) is detectable for 125 stars, and the fourth harmonic is also significant in the spectra of 8 stars. The appearance of higher harmonics suggests that excited non-radial modes are rather non-linear as well.

In addition to the harmonics of the mode frequency, a number of linear combinations with the main pulsation frequency f_1 have been identified. Probable identifications of the combination frequencies corresponding to the period ratios of the horizontal ridges shown in Fig. 3 is given in the last column of Table 5. In some cases, these ridges are formed by several frequencies of nearly equal ratios.

A zoom of the histogram in Fig. 3 around the ratio of 0.61 is show in Fig 4. The distribution show a composite structure: it is either not symmetrical and has two sharp 'side-peaks' as well one at $P_x/P_1 = 0.631$ and the other at 0.593. The frequencies for the 0.631 ratio (hereafter f_{63}) are also known from previous works (Moskalik et al. 2015; Netzel & Smolec 2019). The explanation is also similar to that of f_{61}: $0.5f_{63}$ is the frequency of the non-radial mode $\ell = 8$ and f_{63} is its harmonic. The mode frequency itself ($0.5f_{63}$), and several linear combination frequencies are also common in our sample resulting in clearly visible horizontal ridges in Fig. 3.

The distribution in Fig 4 show a local maximum around 0.62. It must be caused by the frequencies with a ratio of ~ 0.622 isolated by Netzel & Smolec (2019) in the OGLE material. As Molnár et al. (2022) has pointed out, in the mixed metallicity sample of the Galactic field, the individual ridges are less separated than in the case of the much more homogeneous Galactic bulge sample of OGLE. Nevertheless, all three ridges found earlier are clearly identified here, and their centre values remarkably coincide with the values of stars from the Galactic bulge. The frequencies around the ratio 0.62 are explained as linear combination of the two above mentioned non-radial mode frequencies viz. $f_{62} = 0.5f_{61} + 0.5f_{63}$.

In Fig. 5 we show four spectra as a sample in which the f_{61} or f_{63} frequencies are dominant. In the spectrum of panel A, the frequency of the mode $0.5f_{61}$, and its harmonics f_{61}, $0.5f_{61}$, $1.5f_{61}$ and $2f_{61}$ are clearly visible. Some linear combinations of these frequencies with f_1 are also detectable. The position of these detected frequencies are marked with vertical green dashed lines. The spectrum in panel B is dominated by the f_{63} frequency, otherwise the structure is very similar to the spectrum in panel A. Here the identified peaks are marked with a cyan dotted line. The panel C shows a spectrum in which both the f_{61} and f_{63} frequencies are present. The structure

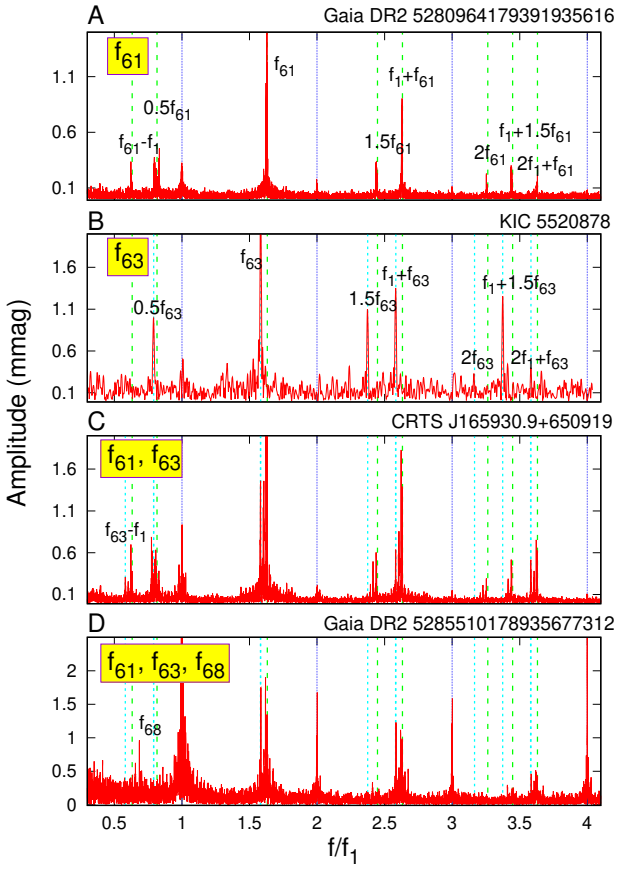

Figure 5. Sample spectra of four stars where f_{61} or f_{63} is the dominant additional frequency. The spectra are pre-whitened with the dominant pulsation frequencies f_1 and their harmonics. The vertical blue lines show the location of these pre-whitened components. Vertical green dashed and cyan dotted lines denote the position of the identified and labeled frequencies in the given panels. For comparison, these vertical lines are redrawn from top to bottom on successive panels. (See the text for the details.)

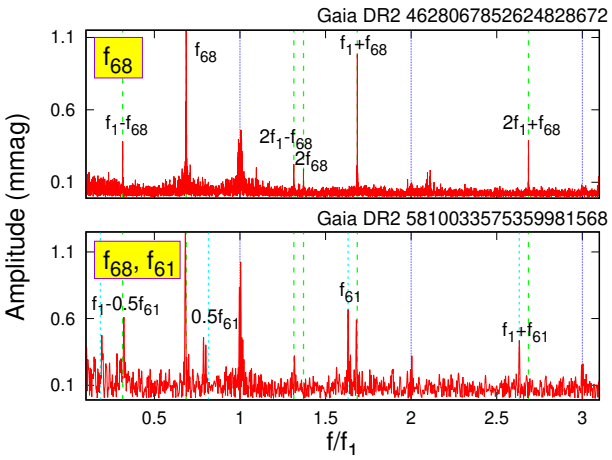

Figure 6. Spectra of two stars where f_{68} is the dominant additional frequency. The structure of the figure is the same as Fig 5.

of the spectrum can be understood as a combination of the spectra of panels A and B. Between the frequencies f_{61} and f_{63}, peaks belonging to the linear combination of the two modes, i.e. f_{62}, $f_{61} + 0.5 f_{63}$ also appear. The star shown in the panel D has, in addition to the f_{61} and f_{63} frequencies, the f_{68} frequency discussed in the next subsection.

4.2.2 *Stars with f_{68} frequencies*

Previous works (e.g. Netzel et al. 2015a; Moskalik et al. 2015; Molnár et al. 2015; Süveges & Anderson 2018) has also identified an independent additional frequency with a relatively large amplitude that is present in many stars. These frequencies have a ratio $P_x/P_1 = 1.459$ or $P_1/P_x = 0.685$ (hereafter signed as f_{68}). Based on analogies, Moskalik et al. (2015) has suggested non-radial g-modes as a possible origin of these low frequencies, but no theoretical modeling has been done on this. Dziembowski (2016) has investigated an other possible explanation for f_{68}, namely, that the stars showing these are not RR Lyrae variables, but low-mass binary 'RR Lyrae impostors' such as OGLE-BLG-RRLYR-02792 (Pietrzyński et al. 2012; Karczmarek et al. 2017). However, he rejected this possibility since such an explanation is contradicted by the existence of stars with f_{68} together with f_{61} frequencies (KIC 9453114 in the *Kepler* field Moskalik et al. 2015, ASAS J213826-3945.0 and NSVS 14632323 in *TESS* data Molnár et al. 2022). Most recently, Molnár et al. (2022) mentioned, but only as an unlikely possibility, a heavily damped $\ell = 1$ mode that causes these frequencies.

The (green) horizontal ridge of f_{68} frequencies clearly visible in Fig. 3. Spectra of 133 stars (21 per cent of the sample) contain frequency with this period ratio. Along with these, we also found a number of linear combination frequencies that contain the f_{68} frequency (see Fig 6). One of these is $f_1 + f_{68} \equiv f_{59}$. These frequencies cause the sharp peak at $P_x/P_1 \sim 0.593$ on the left side in Fig. 4. Previous publications have not reported similar frequencies, however, Dziembowski (2016) shows that the frequencies corresponding to the $\ell = 10$ non-radial mode should be located around here. Is it possible that this is the true mode frequency (precisely half of it) and the mysterious f_{68} frequency is just a simple linear combination (i.e.: $f_{68} = f_{59} - f_1$)?

A search of the Fourier spectra shows that f_{59} frequencies are only found in those 67 stars where f_{68} also appears. This strengthens the connection between f_{59} and f_{68}. In all such cases, f_{59} has a lower amplitude than f_{68}. This suggests that f_{68} is the primary frequency and f_{59} is the linear combination. Although in some special cases, the linear combination frequencies of non-radial modes may have higher amplitudes than their component frequencies (Balona et al. 2013; Kurtz et al. 2015), this is not true for linear combinations with radial modes. This fact is against interpreting the f_{68} frequency as a linear combination. A further argument against the primaryity of f_{59} is that none of the stars containing f_{59} has a frequency corresponding to $0.5 f_{59}$ (the hypothetical frequency of $\ell = 10$ mode).

For at least five stars, the harmonic frequency $2 f_{68}$ was detected (see top panel of Fig 6 for an example). The appearance of higher-order, even fifth-order, harmonics of certain stars' frequencies belonging to the $\ell = 8$ and $\ell = 9$ non-radial modes indicates that non-linear effects also play role in the excitation of these modes (see e.g. Cox 1980). Something similar is suspected from the appearance of $2 f_{68}$ harmonic frequency.

We found 66 such stars with at least one additional frequency (usually f_{61}) besides f_{68}. This further supports the idea that the f_{68} frequencies really belong to RRc stars. What is interesting, however, that linear combinations of f_{68} frequencies with f_{61} or f_{63} frequencies were not found for any stars, even though f_{62} (a linear combination of f_{61} and f_{63}) is so common that it causes a clearly visible ridge in the Petersen diagram shown in Fig. 3. In stars where

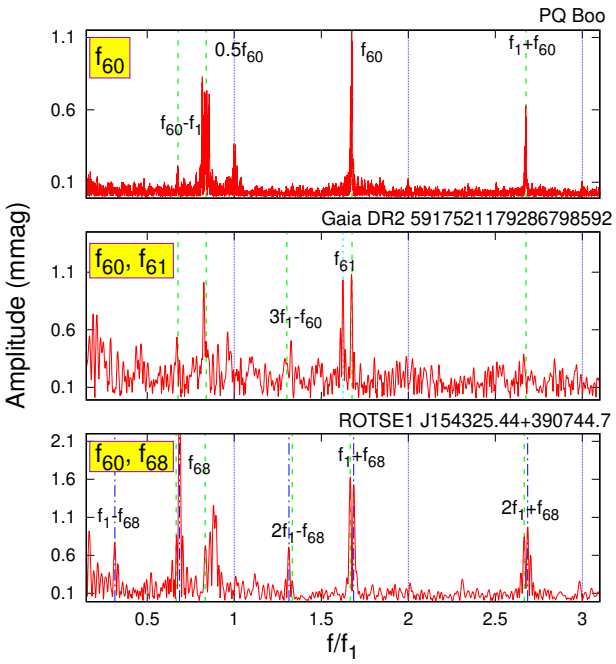

Figure 7. Spectra of stars showing f_{60} frequency and its linear combinations (top); the f_{60} and f_{61} frequencies (middle); or f_{60} and f_{68} frequencies (bottom), simultaneously. The structure of the figure is the same as Fig 5.

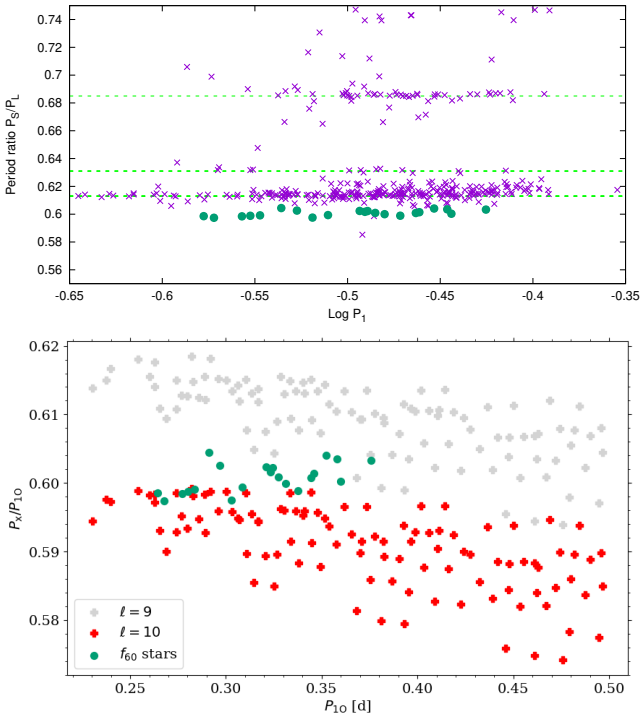

Figure 8. (top) Part of the Petersen diagram. Each symbol represents a star with its dominant additional frequency. Dashed horizontal lines indicate the middle position of the known ridges at 0.613, 0.631 and 0.685, respectively. The stars of the new f_{60} ridge are shown with filled green circles. (bottom) Theoretical models for RR Lyrae stars with non-radial modes of degrees 9 and 10 (see text for details). The stars of the new f_{60} ridge are shown with filled green circles.

both f_{68} and f_{61} are present, f_{61} is almost always dominant, i.e. the spectrum is similar to that in panel D of Fig. 5. There are only eight stars where f_{68} is dominant for at least two sectors (see bottom panel of Fig. 6 for an example). The latter is important because the amplitude of the f_{61} frequency is strongly time dependent (see Szabó et al. 2014; Moskalik et al. 2015 and later in Sec. 5.2). There are several stars where f_{68} dominates in one sector but f_{61} dominates in the following sector or vice versa.

4.2.3 *Frequencies of the $\ell = 10$ modes?*

The histogram in Fig. 3 suggests that in addition to the four frequent period ratios discussed above (which associated with frequencies f_{61}, f_{63}, f_{62} and f_{59}), one more period ratio is relatively frequent in the interval, around 0.602. A frequency with a period ratio between 0.595 and 0.605 was found on 97 stars, 21 of which are the dominant additional frequency. (Hereafter, the frequencies corresponding to this ratio are denoted by f_{60}.)

If we look at the Fourier spectra of stars with these frequencies (see top panel in Fig. 7 for an example), we find that they are similar to the spectra of stars with f_{61} frequencies. Typically, the $0.5 f_{60}$ frequency is also detectable, as well as various linear combinations of the f_{60} frequency and f_1. You might think that these are also f_{61} stars, but for some reason their period ratio is unusually small.

However, this assumption certainly cannot be explained for stars for which the frequencies f_{60} and f_{61} appear simultaneously. Middle panel of Fig. 7 shows the spectrum of such a star. The frequencies associated with f_{60} and f_{61} are clearly separated. For Gaia DR2 5917521179286798592 shown in the figure, the difference between the two frequencies is $\Delta f = f_{60} - f_{61} = 0.185\ \mathrm{d}^{-1}$. This is more than five times higher than the Rayleigh frequency resolution ($0.036\ \mathrm{d}^{-1}$). Frequency splitting might be caused by either amplitude or frequency modulation (Benkő et al. 2011). This is, however, not the case here. The main pulsation is rather stable, as shown from the small residual around harmonics. Using amplitude and phase variation calculating tool of the Period04 package, we also tested the stability of the f_{61} amplitude and phase. We divided the detection period into 2-day slices and determined the phase and amplitude of the frequency for each slice. We obtained that the phase is constant to a good approximation (0.0179 ± 0.0045 rad), while the amplitude shows an wave of $\sim$ 15 days and 0.75 mmag. This variation could explain at most a side peak at a distance of $0.067\ \mathrm{d}^{-1}$. In other words, neither the time variation of the main nor the additional frequency can explain the f_{60} frequency appearing next to f_{61}.

Since the $f_{59} = f_{68} + f_1$ frequency is close to the f_{60}, we also need to show that the f_{60} stars are different from f_{68} stars. There are only few (3-4) candidates where we assume that the f_{59} and f_{60} frequencies appear simultaneously. The best candidate is shown in the bottom panel of Fig. 7. In this case, $\Delta f = f_{59} - f_{60} = 0.06\ \mathrm{d}^{-1}$, which coincides with the instrumental variations that might be caused by the orbital period. This is not possible, however, because in that case the whole light curve would be affected. Additionally, the instrumental origin does not explain the peaks between f_1 and f_{68}, which also appear in all the other similar stars and can naturally be explained by a time-varying and therefore multi-peaked frequency of $0.5 f_{60}$. This type of 'composite' spectrum also appears for simultaneous f_{61} and f_{68} stars (bottom panel in Fig 6).

The upper panel of Fig. 8 we plotted the dominant additional frequency of each star. As can be seen, stars containing f_{60} (green filled circles) are quite distinct from the previously identified f_{61} group (purple 'x' symbols). As mentioned above, there are two possible explanations for this f_{60} group. On the one hand, it is possible that

the stars that make them up define a metal-poor subgroup of RRc stars, and on the other hand, the frequencies associated with the $\ell = 10$ non-radial modes are expected to be somewhere around f_{60} (see Dziembowski 2016).

In the bottom panel of Fig. 8 we compared position of the f_{60} group on the Petersen diagram with theoretical models of RR Lyrae stars with non-radial mode of degree $\ell = 9$ (blue symbols) and $\ell = 10$ (red symbols). Theoretical models were calculated with the warsaw envelope code (Dziembowski 1977) for different values of mass, metallicity, luminosity and effective temperature. The ranges of these parameters are the same as in Netzel et al. (in prep.). We plotted only those models in which both radial first overtone and non-radial mode of a given degree are linearly unstable. To plot period ratios we used harmonic of the non-radial mode, similarly to fig. 4 in Dziembowski (2016). Positions of short-period f_{60} stars are consistent with theoretical models with non-radial mode of degree 10. The f_{60} stars with first-overtone period longer than around 0.32 d are located between the sequences formed by the theoretical models for non-radial modes of degrees 9 and 10.

That is, we get that f_{60} ridge with a shorter period cannot be part of the f_{61} ridge, but the explanation of the $\ell = 10$ ridge in the non-radial mode is plausible. We note that the observed ratios for both f_{61} and f_{63} slightly increase with increasing period, while the models suggest an opposite change.

4.2.4 *Further additional frequencies*

We have investigated what other frequencies occur in addition to those discussed above. The Petersen diagram in Fig. 9 shows the 26 stars whose dominant additional frequency does not fit into the previous categories.

Two groups appear to be distinct: one between 0.706 and 0.776 and another one between 0.85 and 0.896. The first case also includes stars that fall in the sequence of classical RRd stars (black circles). i.e. for these six stars the dominant additional frequency found could be the frequency of the fundamental mode f_0. In Table 2 these stars are denoted by 'f_0?'. Two aspects, however, seem to contradict the classification of stars as RRd variables. (i) For these stars, the amplitude ratio of the two frequencies A_0/A_1 is between 0.032 and 0.019. The smallest such value for classical RRd stars is an order of magnitude larger. (ii) The f_0 frequencies typically appear from a broad forest of peaks. This is the case for all frequencies shown in Fig. 9. The amplitudes and frequencies of the additional frequencies vary over time. This is particularly true for the frequencies of the modes themselves (i.e. $0.5f_{60}$, $0.5f_{61}$, $0.5f_{63}$). The consequence of this is the appearance of side peaks (see Figs. 5 and 7). The amplitude of the side peaks, which may be larger than the main peak, is determined by the actual time dependence (Benkő et al. 2011).

That is, the two groups in Fig. 9 are in fact apparent. For these stars, one of the extreme (right or left) side peaks of $0.5f_{6x}$ is the highest amplitude additional frequency. It should be noted that these stars are not the same as the so-called anomalous RRd stars (Soszyński et al. 2016b), since for all anomalous RRd stars the f_0 frequency is dominant compared to f_1. They are also different from the new group described by Prudil et al. (2017), since the inverse period ratio ($P_x/P_1 = f_1/f_x$) of their stars falls in this part of the Petersen diagram.

4.2.5 *Additional frequencies and the Fourier parameters.*

Fig. 2 shows not only that the Fourier parameters of our sample coincide with those of the RRc stars, but also that the parameters of the

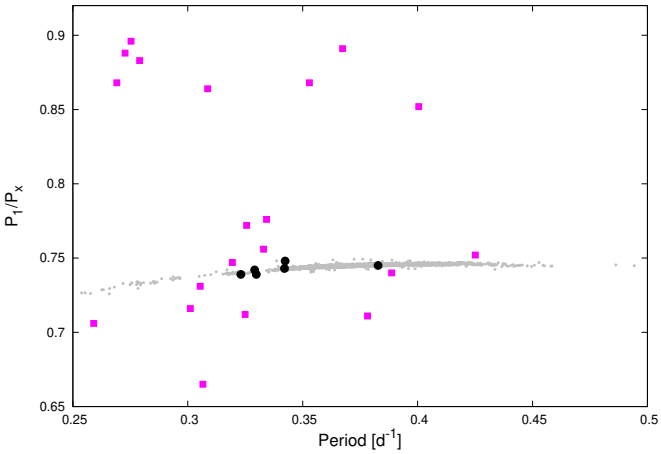

Figure 9. Stars with a dominant additional frequency ratio f_x/f_1 between 0.7 and 0.8. Filled black circles indicate the possible RRd stars. Grey dots show stars of the OGLE RRd sample (Soszyński et al. 2014).

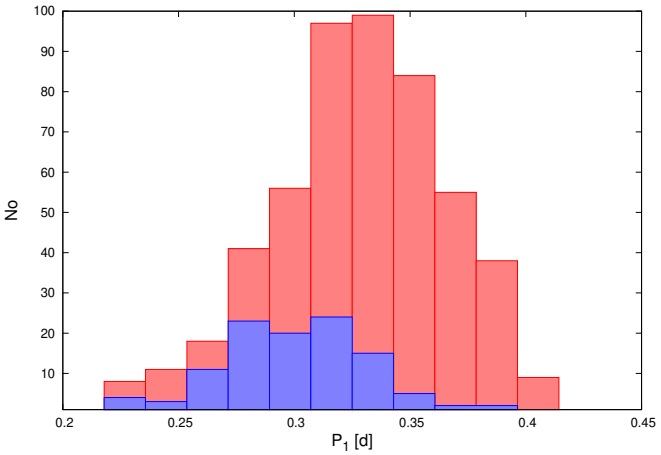

Figure 10. The number of stars that show (red boxes) and those that do not show additional frequencies (blue boxes) as a function of the main period.

stars with additional frequency (red symbols) and those without (blue symbols) are somewhat different. This shows that there might be a physical difference between the two groups, and that we do not detect additional frequencies in certain stars not only for observational reasons.

The obvious feature is that while the extra-frequency star occurs over the whole parameter range, the stars without extra frequency almost all fall in the shorter period ($P < 0.35$ d) range. The phenomenon is illustrated by the distribution of stars in Fig. 10. In each period bin, stars with detectable additional frequency are in the majority, but stars that do not show such frequency are concentrated in the shorter periods and almost absent in the longer period bin. Or, in other words, the ratio of those stars that do not show an additional frequency to those ones that do decreases as the period increases.

Recently, Netzel & Smolec (2022) have derived theoretical models to determine the parameters under which the $\ell = 8$, $\ell = 9$ and $\ell = 10$ non-radial modes can be excited in the overtone pulsating RR Lyrae stars. Excitation of all three non-radial modes is possible over a wide range of metallicities over most of the instability band. However, as the blue edge of the instability strip is approached, the excitation of the $\ell = 8$ and then the $\ell = 9$ non-radial modes is also no longer presented (see fig. 2 in Netzel & Smolec 2022). That means among the hottest RRc stars, there are more likely to be stars that do not

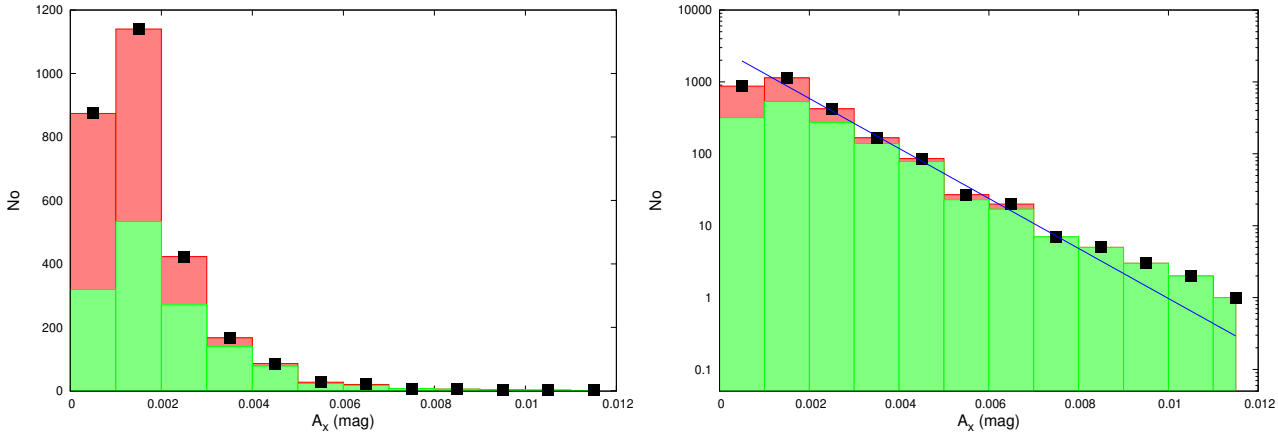

Figure 11. Amplitude distribution of 0.61 additional modes. The number of found additional frequency as a function of its amplitude in normal (left) and in logarithmic (right) scales. Green columns show the frequencies in 0.61 sequence, while red ones indicate all frequencies between $P_S/P_L = 0.55$ and 0.65.

excite non-radial modes. This phenomenon is also manifested in the fact that if the possible $\ell = 8$ or $\ell = 9$ regions are plotted on the Petersen diagram (see fig. 3 in Netzel & Smolec 2022), they are wedge-shaped: longer periods allow a wider period rate than shorter periods for the excitation of these non-radial modes. Comparing this with what we found from the observations, we can say that the theoretical prediction and the measurements, at least at a qualitative level, gave similar results.

That stars without an additional mode are more frequent among shorter-period RRc was shown not only by the smaller *TESS* sample of Molnár et al. (2022), but also by the stars of Jurcsik et al. (2015) in the globular cluster M3, but it became evident with the present larger *TESS* sample. The phenomenon supports that the theoretical explanation for the additional frequencies is correct.

4.2.6 *Amplitude distribution*

For comparison, the amplitude distributions of the additional frequencies were calculated in a similar way as done by Netzel & Smolec (2019): we considered the frequencies either between 0.6 and 0.62 (f_{61} stars), and also the frequencies between 0.55 and 0.65. We plotted in Fig. 11 the number of additional frequencies found as a function of their amplitude for these two cases. Both cases the distributions are very similar to each other and to the similar plots prepared to the OGLE sample (see fig. 4 and fig. 5. of Netzel & Smolec 2019). The red boxes disappear at high amplitudes in Fig 11. This means that f_{63} have typically lower amplitudes than f_{61} frequencies. For values larger than 0.01 mag amplitude, the distribution appears similar to an exponential one, while for smaller amplitudes, there is a deficiency compared to the exponential distribution. The relatively smaller number of frequencies with small amplitudes would be understandable at first glance, since the smaller the amplitude, the less likely we are to detect them.

However, the logarithmic scale plot shows another difference from the exponential distribution: we detect more frequencies with large amplitudes than we would expect from such an exponential distribution. To illustrate this phenomenon, we constructed a data series from our four sequence histograms (black rectangles in Fig. 11). The central part of the logarithmic version of the data set (between $A_x = 0.0015$ and 0.008 mag) was linearly fitted (blue line). The fit of the line is excellent (rms=0.18), towards higher amplitudes the excess in the number of detected frequencies is evident.

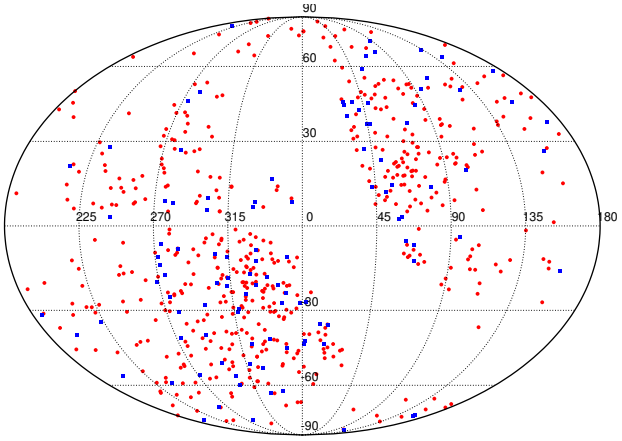

Figure 12. Galactic distribution of the bright *TESS* RRc sample. Red dots: stars with additional modes, blue rectangles: stars without additional modes.

Using 'FindDistribution' tool of the MATHEMATICA program package (Wolfram Research, Inc. 2021), we searched for the distribution that best fits our data set. The solution is, however, the 'empirical' distribution. The Zipf distribution (see e.g. Johnson et al. 2005) suggested as second possibility gives worse fit than the above exponential one. If we search for a distribution by adding to the first element of the histogram the 109 stars in which no additional frequencies were found, i.e. assuming that the additional frequencies are of such small amplitude that we could not detect them, the result is the same. All we can say is that the amplitude distribution of the additional frequencies is exponential over a wide range, but there is a deficit for the lowest amplitudes and a surplus for the highest amplitudes.

4.2.7 *Distribution in space*

In subsection 4.2.5 we saw that stars that do not exhibit the additional mode are different from those that do: they have typically a shorter period. What is the distribution of these stars in the Galaxy?

In Fig. 12, we have plotted our stars in galactic coordinates. The red dots represent stars that show the additional mode(s), while the blue rectangles show stars that do not. We examine whether there is a difference in the spatial distribution of stars with and without additional modes. To this purpose, a two-dimensional two-sample

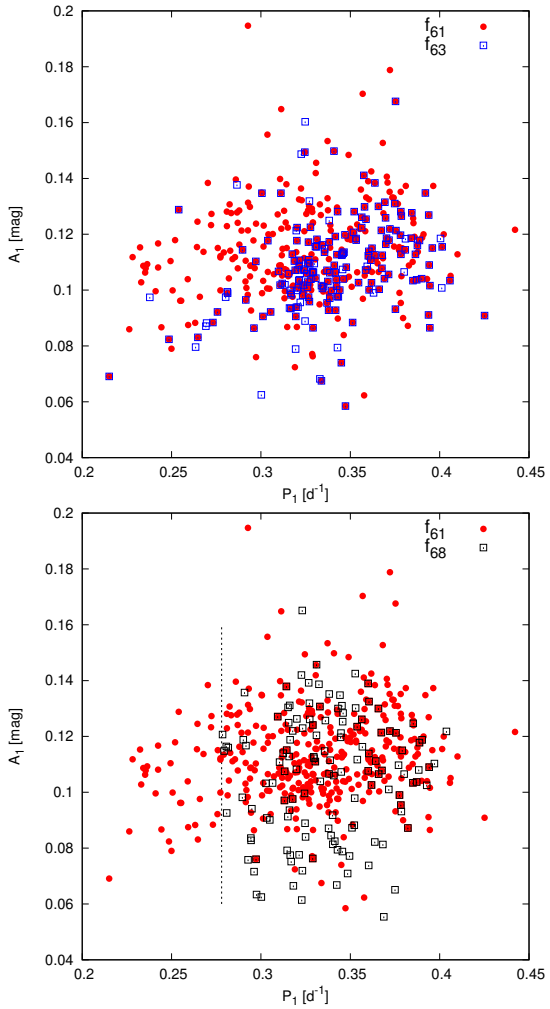

Figure 13. Appearance of the f_{61} and f_{63} additional frequencies as a function of P_1 (top). Filled red circles and empty blue rectangles show the positions of stars which have either f_{61} or f_{63} frequencies. Many stars show both. Stars with f_{61} and f_{68} frequencies (bottom). Red points are the same as above, while empty black rectangles represent stars with f_{68} frequency.

Kolmogorov–Smirnov (KS) test (Press & Teukolsky 1988) was applied to the coordinates of the two sets of stars. The two-sample KS test does not make any assumptions about the actual shape of the distributions, but only measures whether or not the two data distributions can be from the same distribution. As Press & Teukolsky (1988) has shown if the test result probability p_r is larger than 0.20 then the assumption that the two data distributions are not significantly different is certain. In our case $p_r = 0.487$, so we can conclude that the spatial distributions of RRc stars with and without additional modes do not differ.

4.2.8 *Distribution of additional frequency types*

In Sec. 4.2.5 we saw that the distribution of stars that do and do not show an additional frequency, regardless of its type, differs in the space of Fourier parameters. We also saw in Sec. 4.2.3 that f_{60} stars could be excited anywhere thorough the instability strip even at short periods, and in our sample the period distribution appears to be relatively even. In any case, the number of elements in our f_{60} sample is small to make any sharp statement. What about the distribution of other types?

In the top panel of Fig. 13 we plotted the stars showing f_{61} (filled red circles) and f_{63} (empty blue rectangles) additional frequencies as a function of P_1. The vertical scale show the amplitude of the main period A_1. An evident structure can be recognized in the figure: stars with shorter periods and higher amplitudes typically show only f_{61}, while stars with lower amplitudes and longer periods typically show both f_{61} and f_{63} frequencies. If we look at the theoretical HRD of Netzel & Smolec (2022), we see that there is indeed a range where only the $\ell = 9$ non-radial mode can be excited, but not the $\ell = 8$. This range is, however, rather narrow. As shown by Bellinger et al. (2020) the amplitude of the light curve and the period are the two most important parameters that determine the effective temperature of RR Lyrae stars. However, this is only a correlation, not a simple function, since luminosity, mass and chemical composition also play an non-negligible role (see e.g. Marconi et al. 2015 and further references therein). To make a quantitative comparison between the theory and observation would require a deeper analysis, which is beyond the scope of this paper.

In the bottom panel of Fig. 13 we show with red filled circles the same f_{61} stars as in top panel while the black empty squares denote the stars containing f_{68} frequencies. A sharp threshold is visible here (dashed vertical line in Fig. 13). No star with a period shorter than 0.278 days was found to have an f_{68} frequency. This cut-off seems to be a peculiarity of our sample, as both in OGLE and *Kepler* data have several stars with a period shorter than 0.278 d and yet have f_{68} in their spectra (Netzel et al. 2015a,b; Moskalik et al. 2015).

5 STARS AROUND THE CONTINUOUS VIEWING ZONE

Around the ecliptic poles, all stars are continuously observed by *TESS*. That means we have a year's length of data series. Time series of this length provide an opportunity for other types of studies in addition to those discussed above.

5.1 Stability of the main frequencies

The period variation of RR Lyrae stars has long been a core topic of research on these stars. Investigating of long data series, sometimes centuries long, has shown that fundamental mode pulsating (RRab) stars, which do not show the Blazhko effect, are characterized by a continuous, slow period change, which is compatible with stellar evolution models. On the other hand, RRab stars with Blazhko effect have much stronger periodic variations and are typically irregular in nature (Le Borgne et al. 2007; Jurcsik et al. 2001, 2012; Szeidl et al. 2011). The rates of these period changes are several orders of magnitude higher than the predicted rates of stellar evolutionary theories.

The situation with RRc stars is a bit different. Besides the continuous period changes of stellar evolutionary origin, quasi-periodic and irregular changes were detected also for non-Blazhko stars as well. Latter variations are particularly common among RRc stars with longer main periods (see e.g. Jurcsik et al. 2001, 2012; Percy & Tan 2013 and further references therein).

The physical background of the long time-scale and strong period changes of RR Lyrae stars is still unknown. For few (quasi)periodic cases, binarity has been raised as a possible explanation (Derekas et al. 2004; Sódor et al. 2017; Li et al. 2022), but there are many arguments against it, not to mention irregular changes, which certainly cannot be explained by binarity. Since the stellar pulsation is not a strictly repetitive phenomenon, accumulating random phase variations can cause both quasi-periodic and irregular O−C (observed

minus calculated) diagrams (see Sterken 2005 for a review). This random walk explanation is plausible, and it was raised a long time ago (Balázs-Detre & Detre 1965). The problem is that the magnitude of the recently verified cycle-to-cycle random variation of the light curve is much smaller than could explain the observed diagrams (Derekas et al. 2012; Benkő et al. 2019). An explanation based on a similar principle is when the pulsation period fluctuates periodically or quasi-periodically around an average. In this case, similar (quasi-periodic or irregular) O−C diagrams could be obtained (Sterne 1934; Lombard & Koen 1993). This idea can explain the behaviour of the O-C diagrams of Blazhko RR Lyrae stars, but not for RRc stars that do not show the effect.

Additionally, numerous RRc stars show a short time-scale 'phase jump' (e.g. Wils et al. 2007; Wils 2008; Odell & Sreedhar 2016; Berdnikov et al. 2017; Benkő et al. 2021). This means that, when constructing the phase diagram, phase jumps over time must be assumed for folding the curves properly, but the shape of the light curve is not changed. This feature makes it unlikely that the phenomenon is caused by a long-period Blazhko effect, since in that case there would be a correlated change in amplitude and phase. Similar phase jump phenomena have not been reported for RRab stars.

The investigation of the details of the phase jump phenomenon was not possible in the past, since for this purpose, continuous time series are needed. The first opportunity to study this effect was the *Kepler*'s 4-year continuous measurements. These suggest that the phase changes occur with a few hundred days of continuous variation and not a sudden jump (Moskalik et al. 2015; Sódor et al. 2017). In other words, it seems that the phase jumps are just a manifestation of fast period changes.

During its original mission, the *Kepler* space telescope observed five RRc stars continuously for 4 years. *TESS* has given us the opportunity to extend the study to a larger sample, as stars around the ecliptic pole have been measured continuously for about a year. We selected stars from our sample that were observed by the space telescope in at least 10 sectors. This resulted in 32 stars for us: 17 in the southern and 15 in the northern hemisphere.

5.1.1 Phase variation functions

In a study on *Kepler* RRab stars has been shown that the information content of the phase variation function is the same as that of the O−C curve (Benkő et al. 2019). Thus, for investigating phase/period variations of RRc stars on an annual time-scale we constructed their phase variation functions by a template fitting method. To our knowledge, such method was first used for this purpose by Jurcsik et al. (2001), who demonstrated its higher sensitivity than the classical O−C analysis. Template fitting algorithms were subsequently used as an alternative to O−C analysis in a number of publications (e.g Derekas et al. 2012; Li & Qian 2014; Benkő et al. 2016, 2019).

The specific algorithm we used defines a template for each star by using the Fourier solution of the complete data set with the main pulsation frequency f_1 and its n harmonics. Then it splits the data for cycles and fits the template to the first data slice containing n_s cycles. In the next step, the starting point of the slice to be fitted is shifted by S cycles, and then this process is continued until the end of the data series. The fit has three free parameters: the phase, amplitude and zero point of the light curve. We stress that we are not concerned with Fourier amplitudes and phase, but with global parameters. The actually used parameters were: $n_s = 5$, $S = 3$ and $n = 10$, for the number of pulsation cycles to be fitted in one step, the steps-size in number of pulsation cycle, and the maximal number of harmonics to be used in the template, respectively. These parameters were not optimal for TYC 8896-623-1 and Gaia DR2 4654252618960823936, for which we used $n_s = 10$.

To find the optimal values of the aforementioned global parameters in case of each light curve chunk, we used `scipy`'s `curve_fit` method (Virtanen et al. 2020). The fittings were performed using the trust region reflective algorithm. The errors of the parameters were calculated from the diagonal of the estimated covariance matrix returned by `scipy`.

The panels of Fig. 14 show the relative phase variation $\Delta\phi$ as a function of time for all 32 stars (red symbols) and the simultaneous change in relative amplitude $\Delta A(t)$ (light blue symbols). From each $\phi(t)$ phase change curve, we subtract a fitted linear. This step both corrected for any inaccuracy in the period (which would cause a linear trend in the plots) and shifted the curves to a common mean of zero. We called the resulting $\Delta\phi$ as relative phase. In order to transform the amplitude to a common scale as well, we subtracted the average amplitude $\langle A \rangle$ from the amplitude change functions. These became the relative amplitudes $\Delta A(t) = A(t) - \langle A \rangle$.

Looking at the long-scale behavior of the curves, we can distinguish the following types: (1) constant phase and amplitude, (2) annual-scale change in the phase but no significant amplitude change, (3) correlated periodic variation both in amplitude and phase. In addition to all this, (4) smaller amplitude and shorter period phase (and amplitude) fluctuation is also seen in the curves of many stars.

The Case 1 (see e.g. stars Gaia DR2 5486632674089049472 or GSC 04450-00308 in Fig 14) does not require further explanation. These stars have stable period and amplitude.

The behavior of the stars in Case 2 is similar to KIC 4064484 and KIC 9453114 studied by Moskalik et al. (2015) and to KIC 2831097 found later by Sódor et al. (2017). Namely, a phase change of high amplitude and long period is seen in the stars. The period, if it is a periodic signal at all, is longer than the observation time span (see e.g. HD 270239, Gaia DR2 5285510178935677312, Gaia DR2 1650042086261498880, or CRTS J165435.7+655131). For other stars the shape of the curve is even less pronounced to be periodic (e.g. CRTS J165930.9+650919, CRTS J165523.7+573029). Since this long timescale phase variation does not associated with a similar type of amplitude change, these stars unlikely to be long-period Blazhko stars. The variations we are seeing here are probably no more than the actual course of time the phenomenon which appeared in previous ground-based observations as seasonal phase jumps.

When we detect an amplitude variation correlated with the phase variation, and the period of these variations are much longer than the main period (Case 3), we are faced with the classical Blazhko effect by definition. Such stars are: Gaia DR2 4676321123000662272, Gaia DR2 4654252618960823936, TYC 8896-623-1, NSVS 2852763, V420 Dra and XX Dor. Six stars from this 32-element, or 18.7 per cent of the sub-sample. Consecutive Blazhko cycles are usually not identical, indicating the presence of more than one periods (see e.g. Gaia DR2 4654252618960823936, NSVS 2852763, V420 Dra). The frequent multiperiodicity of the Blazhko phenomenon has been demonstrated for *Kepler* RRab stars (Benkő et al. 2014), i.e. there is no difference in this respect between the Blazhko effect of fundamental mode and overtone stars.

Let us turn to Case 4. With such quasi-periodic phenomena, there is always the question of whether we are dealing with some kind of instrumental noise. For this reason, we emphasize that the phenomenon is perhaps even clearer in the phases, which are much less sensitive to instrumental problems, since they are primarily related to time measuring. In Fig. 14, the additional frequencies found in the star are marked in the upper right corner of the pan-

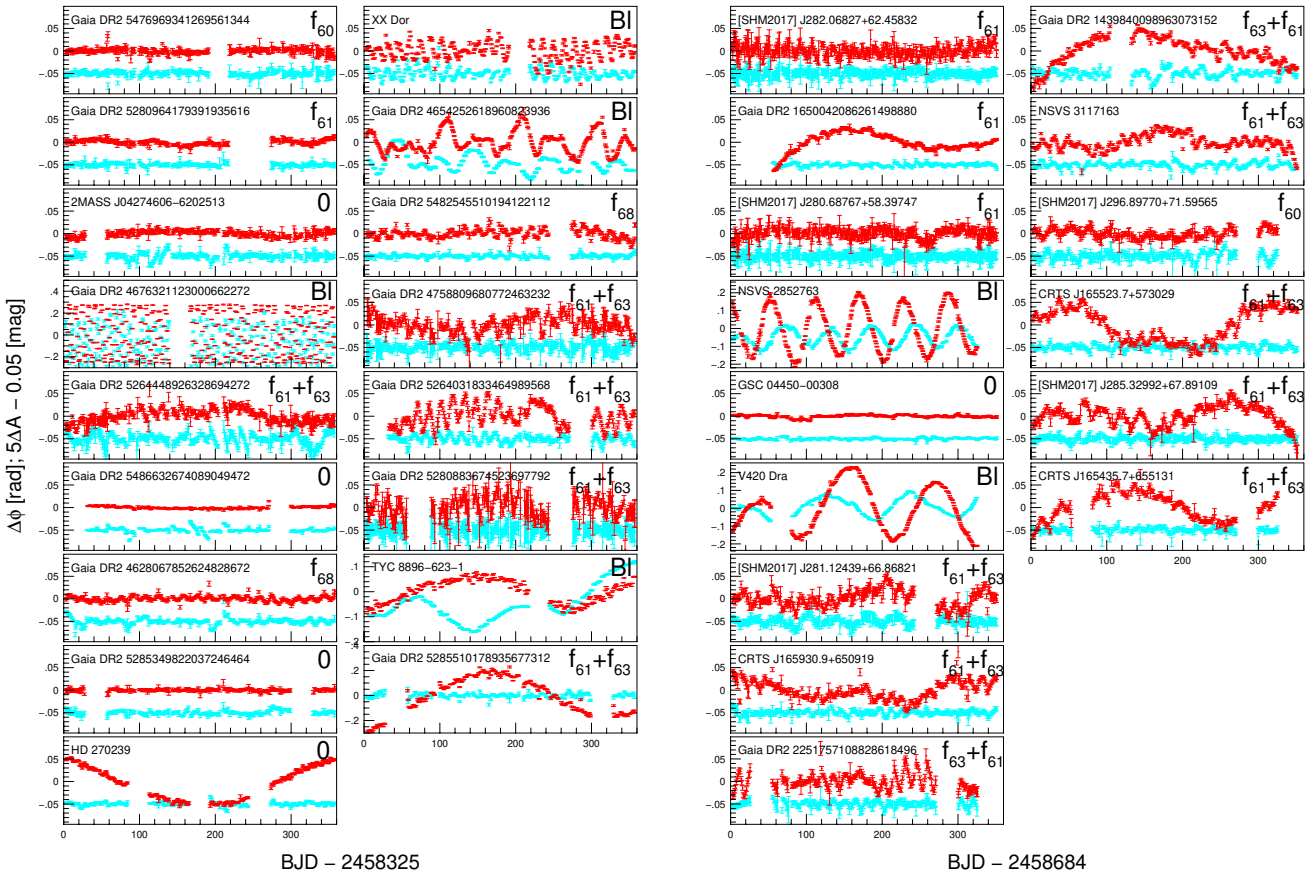

Figure 14. Relative phase variation $\Delta\phi(t)$ of the *TESS* RRc stars's around the ecliptic poles. The light curves observed almost continuously for a year. The stars of the southern hemisphere contain the two columns of panels in the left, while the northern stars show the two columns in the right. The stars are arranged according to the main pulsation periods from top to bottom and from left to right. The time span is the same for all stars and fitted to the longest data sets as 358 days. The horizontal scales are also the same (0.2 rad) for most of the stars, except Gaia DR2 4676321123000662272, TYC 8896-623-1, Gaia DR2 5285510178935677, NSVS 2852763 and V420 Dra where larger scales are needed. For comparison, the relative amplitude variation $\Delta A(t)$ is also shown with light blue symbols in the same (0.2 mag) scale. For better visibility, $5\Delta A - 0.05$ have been plotted.

Table 6. Frequencies in phase variation function spectra (northern sky sorted by the main period according to Fig. 14)

Name	Freq. d^{-1}	S_f	Err. d^{-1}	ident.	p_I
[SHM2017] J282.06827+62.45832	0.07098	12.51	0.00081	i?	0.7858
	0.06761	9.64	0.00092	i	0.9960
	0.43823	5.85	0.00118		
	0.00682	5.59	0.00121	i	1.0000
	0.00332	10.75	0.00087	i	1.0000
	0.13163	5.62	0.00120		
	0.29157	6.02	0.00116		
	...				

The full-size table is available in machine-readable format in the electronic supplement.

els. There is a clear correlation between the strength of the this type of fluctuation and the number of exited addition modes. The most stable stars are those which have no extra frequencies (marked by '0' in Fig. 14), then they followed by those with one mode ($\ell = 8$, $\ell = 9$, or $\ell = 10$). Stars with two simultaneously exited ($\ell = 8$ and $\ell = 9$) non-radial modes have generally the highest phase (and amplitude) fluctuation. The appearance of f_{68} also causes some fluctuations (see: Gaia DR2 4628067852624828672 and GaiaDR2 5482545510194122112), but to a much lesser amount than f_{61} or f_{63}. One aspect of this phenomenon has already been reported in the work of Moskalik et al. (2015), namely, that the amplitude variation of f_{61} frequency over time is accompanied by the amplitude variation in the main frequency over time. Because of our larger sample, it became clear that this phase (and amplitude) fluctuations are caused by the appearance of additional mode frequencies, or more precisely, their variation over time.

In Fig. 14, the stars of the two hemispheres are sorted separately according to their main period. Apart from the Blazhko stars, there

is a tendency that stars with longer periods show phase fluctuation more frequently than shorter period stars. This is more evident from the left two panels in Fig. 14 (southern hemisphere stars). This is the same phenomenon that we have already discussed in the Sec. 4.2.8: the f_{61} and f_{63} frequencies together typically appear in stars with longer periods (see also Fig. 13).

As we mentioned above, the same kind of tendency has previously been published between the large-scale irregular changes in the O−Cs over decades and the main pulsation period. This raises the hypothesis that we have already found the explanation of O−C behaviour of non-Blazhko RRc stars: the phase fluctuations of the main period caused by the variation in the additional frequencies are summed up in the O−C diagrams. In other words, non-Blazhko RRc stars that show strong O−C variation are most likely excited by at least one, but more likely two, non-radial modes. And stars that do not show such O−C variations are likely to have no non-radial modes present. A detailed discussion of the topic will be given in a separate paper.

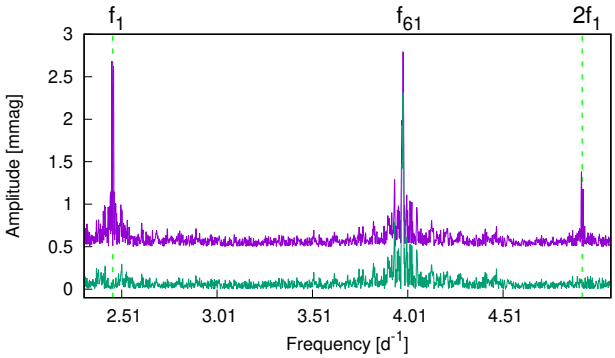

Figure 15. Pre-whitened spectra of CRTS J165435.7+655131 between f_1 and $2f_1$. The upper (magenta) line is the spectrum of the original light curve (shifted by 0.5 mmag for better visibility), while the bottom (green) line shows the spectrum of the line curve from which we have subtracted the time variation of the main period.

5.1.2 Frequencies in phase variation functions

For qualitative results, all phase and amplitude variation curves were subjected to a Fourier analysis using again the SigSpec program package. The program continuously pre-whitens the Fourier spectrum with the frequency of the highest significance until it finds a significant ($S_f > 5$) frequency. The frequencies found in phase variation curves are listed in Table 6. After the name (column 1) we show the frequencies (col. 2) their spectral significance (col. 3) and their estimated 1σ error (col. 4). The accuracy of the frequencies obtained from a discrete Fourier analysis is not a simple task. In a semi-empirical study, Kallinger et al. (2008) demonstrated that the value $\sigma_K = 1/(T\sqrt{S_f})$ is a reliable upper estimate for the frequency determination error so we used this estimate in this section. (Here T is the total time span of the observation.) These σ_K values are given in col. 4 of Table 6. In our case these values are between 0.00032 and 0.00147 d^{-1}. The remark column of Table 6 contains possible identifications of the frequency. Since the amplitude is sensitive for technical issues we does not discus the Fourier spectra of amplitude variation in detail. We just noted by an asterisk here in column 5 if the given frequency is significant in the spectrum of the amplitude change curve as well.

The spectrum of star Gaia DR2 5285349822037246464 contains no significant frequency but for all other stars 2–15 significant frequencies have been found. In total, 203 frequencies were found in the 32 stars. Many similar frequencies appear on different stars. Some of these are certainly not of stellar but technical origin (e.g. caused by inappropriate stitch of sectors, instrumental trends, data length etc.). The critical point is in which cases two frequencies can be considered identical. If the difference between two frequencies from different stars is less than $1\sigma_L$ (where σ_L is the higher standard deviation of the two frequencies), then they should be considered identical. If we have such a sense identical frequencies (possibly from more than two stars), it is suggested that these could be technical frequencies.

We selected those f frequencies that could be detected on at least two stars as possible technical frequencies, and then estimated the numerical probability that they are. The Nyquist frequency f_N of the phase curves of each star varies (depending on the period) between 0.666 and 0.412 d^{-1}. The distance of possible pairs of frequencies found for a given star at a frequency f: $\Delta f^{(1)} = |f - f^{(1)}|$, $\Delta f^{(2)} = |f - f^{(2)}|$, ... After some elementary considerations, we obtain the probability that for a given frequency there are k different frequency pairs within the σ_L error ($\Delta f < \sigma_L$ for all cases) of it:

$$p = \prod_{j=1}^{k} \sum_{i=0}^{m-2} \frac{\Delta f^{(j)}}{f_N^{(l)} - i\Delta f^{(j)}}, \qquad (2)$$

where m and l are integers and denote either the total number of found frequencies in the given hemisphere ($m = 119$ for northern and 84 for southern sky) and the index of the given star, respectively. The value of $p_I = 1 - p$, the probability that a given frequency is instrumental in origin, is shown in column 6 of Table 6. If $p_I \geq 0.99$, we considered the frequency to be instrumental (sign 'i' in col. 5 of Table 6). We identified 113 such frequencies (56 per cent). If $0.99 > p_I > 0.51$ then it is possible that the frequency is instrumental and an 'i?' mark is shown in the table. An additional 48 such frequencies were found. Based on the fact that they appear in the spectra of several stars, 161 (79 per cent) of the total 203 frequencies found could be instrumental in origin.

Of course, this is an upper estimate, since intrinsic frequencies can also coincide with each other or with instrumental frequencies. For instance, the long time-scale phase variation (Case 1 and Case 2) can formally be described by a few low frequencies and such frequencies can really be detected for all these stars. However, these frequencies are primarily determined by the length of the data series, and as such are considered technical frequencies.

On stars showing the Blazhko effect (Case 3), the Blazhko frequency (and sometimes its harmonics) can be detected. The multi-periodic cases were also reflected in the spectra: more than one significant Blazhko frequency could be identified.

The low amplitude and higher frequency fluctuation in the curves (Case 4) yield the most significant frequencies. The characteristic time of these fluctuations is a few days which often makes it difficult to separate them from variations of technical origin such as satellite orbital period (13.7 d) or sector length (~ 27.4 d). Typically, there are several similar frequencies in the phase variation curve of a single star. The appearing of close frequencies explains the beating phenomenon observed in several stars (see i.e. Gaia DR2 5264031833464989568, Gaia DR2 2517571088286184 96). This strengthens that these variations are quasi-periodic.

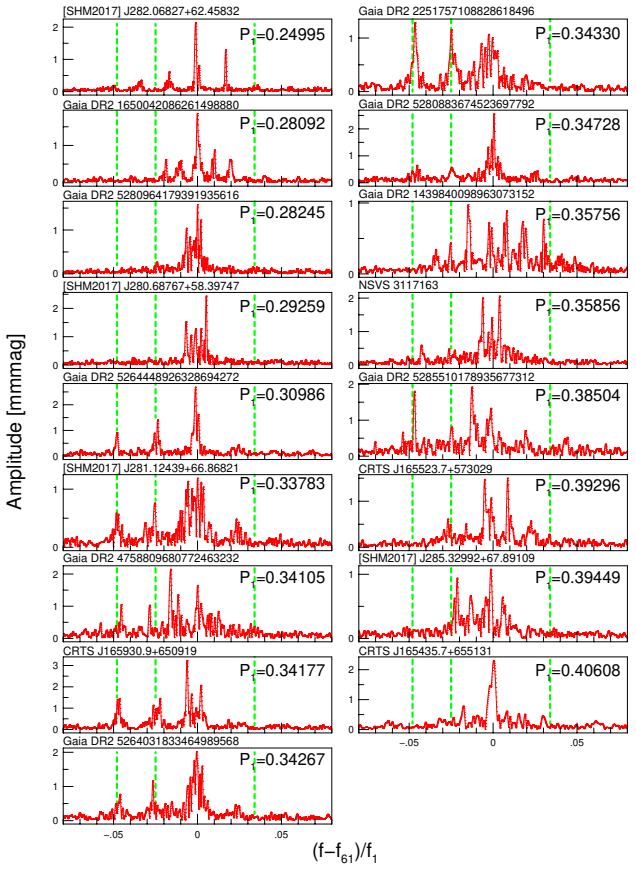

Figure 16. Fine structure of the pre-whitened spectra around the additional frequency f_{61} after the main frequency variations have been transformed out. For comparison, the horizontal scale is normalized by the main frequency. The vertical green dashed lines from left to right show the possible average position of the frequencies f_{63}, f_{62} and f_{60}.

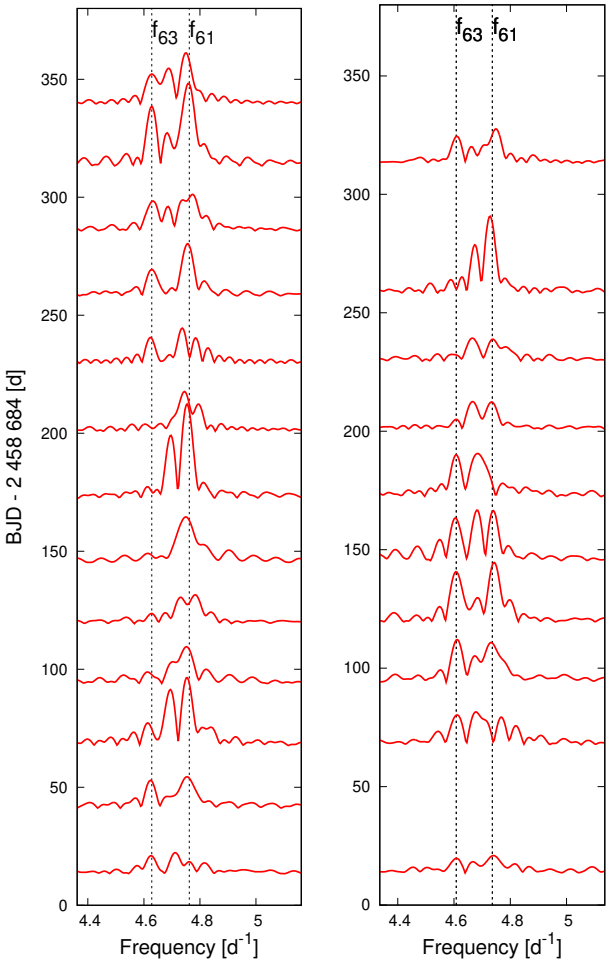

Figure 17. Time variation of the spectrum around f_{61} and f_{63} frequencies. left: CRTS J165930.9+650919, right: Gaia DR2 2251757108828618496. The dashed vertical lines show the position of the average frequency of f_{61} and f_{63}, respectively.

5.2 Time variation of additional modes

As we have seen above, for most stars, the amplitude and phase of the main period vary in time. This means that before we study the time dependence of the additional frequencies, we need to separate this variation, otherwise we would see a mixture of two effects. The time dependence of the main pulsation appears in the Fourier spectra as peaks around the main frequency and its harmonics, which remain in the residual spectrum after a standard pre-whitening step. Moskalik et al. (2015) solved the problem by introducing time-dependent Fourier analysis. Here we have chosen a less sophisticated, but still working method: we have subtracted from the light curves the amplitude and phase variation curves of Fig. 14, and then analysed the residual light curves. In practice, the amplitude and the phase modulation and the zero point curves are binned to 30 points and then interpolated to the original times. This makes easier to track the complex long-period variations than, for example, a polynomial fitting. The efficiency of our method is shown in Fig. 15, where we present the pre-whitened spectrum of the original and corrected light curves of a typical star. The residuals around kf_1 are almost completely disappear from the corrected data series.

From the corrected data series, we selected those that contain the f_{61} frequency but do not show the Blazshko effect. Fig. 16 shows the pre-whitened spectra of these stars around the frequency f_{61}. The stars are sorted by their main period in ascending order from top to bottom. Starting with the shortest period star, we see that in the first 3-4 cases, as the main period P_1 increases, the modulation period of the f_{61} frequency also increases. (This is shown by the fact that the modulation side peaks are getting closer and closer to the main peak of f_{61}. The positions of the frequencies associated with other modes are marked with vertical green lines to separate them from the side peaks.) This is the opposite of what Moskalik et al. (2015) found for *Kepler* RRc stars. If we continue to examine the spectra with increasing main period, we find that (i) the f_{63} frequency appears from Gaia DR2 5264448926328694272 (leftmost peaks), and (ii) the distance to the side peaks around the f_{61} peak does not decrease continuously. Point (i) is in agreement with the picture obtained in Sec. 4.2.8: RRc stars with longer periods typically excite both $\ell = 8$ and $\ell = 9$ non-radial modes. While the point (ii) indicates that there is no direct relationship between the variation period of the f_{61} frequency and the main period. The trend reported by Moskalik et al. (2015) is rather a small sampling effect.

The f_{61} and f_{63} frequencies appearing on the same star seem to vary differently in time because the structure of the side peaks around them is different. This is particularly evident for stars e.g. CRTS J165930.9+650919 or Gaia DR2 2251757108828618496. In Fig. 17 we show the time evolution of the Fourier spectra of these two stars around the frequencies f_{61} and f_{63}. The spectra were calculated for each sector separately and plotted by shifting the spectra by the

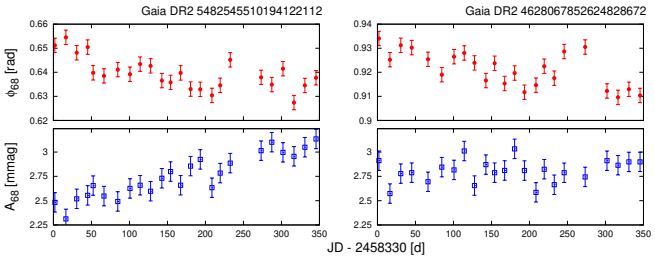

Figure 18. The phase (Φ_{68}: filled red circles) and amplitude (A_{68}: empty blue rectangles) variation of the f_{68} frequency on the two non-Blazhko stars observed in the CVZ.

midpoint of the observation time of each sector. It is clearly visible how the amplitude and frequency (phase) of f_{61} and f_{63} vary over time. In both cases shown here, but also in general, the frequency variation of f_{63} is much smaller than that of f_{61}. The amplitude of f_{61} frequencies vary in shorter time scales than the f_{63} frequencies which could already be seen from the side-peak structures in Fig. 16.

The time dependence of the f_{68} frequency has not been investigated in details so far, although Netzel & Smolec (2019) noted that the frequency is coherent: "Amplitudes and phases of these signals do not vary in time." We have two non-Blazhko stars in the CVZ, which show the f_{68} frequency (Gaia DR2 5482545510194122112 and Gaia DR2 4628067852624828672). We split the corrected and pre-whitened residual light curves based on the gaps in them, and thus calculated amplitudes and phases on data series of roughly one orbit length with Period04. The results are shown in Fig. 18. The amplitude and phase of the f_{68} frequency of Gaia DR2 5482545510194122112 varies in an anti-correlated manner. The variation is small in both cases: $\sim$ 0.02 rad in phase and $\sim$ 1 mmag in amplitude. For Gaia DR2 4628067852624828672, the phase change is again on the scale of 0.02 rad, but the amplitude is constant within 3σ error. Based on these two stars, we suspect the f_{68} frequencies may also vary but at least one order of magnitude lower in amplitude than the f_{61} frequencies, while the phase variations are at least two orders of magnitude lower. For a more definite statement, a larger sample (e.g. several seasons of *TESS*) needs to be investigated.

If we look at the spectra of Blazhko stars that contain the f_{68} frequency, we see that Blazhko side peaks also appear around the f_{68} frequency (see Fig. 19). For the V420 Dra, the $2f_{68}$ harmonic is not even significant, only the right Blazhko side peak ($2f_{68} + f_B$) is visible in the spectrum (the situation is similar for NSV 2852763). The influence of the Blazhko effect on the f_{68} frequencies further strengthens that these are in fact the frequencies of RRc stars.

6 SUMMARY

We analysed the space photometric observations of a Galactic field RRc sample observed by *TESS* satellite. Our main findings related to the main pulsation of stars:

(i) We found an incidence rate of 10.7 per cent for the Blazhko effect. This is consistent with the results of previous works on different subsystems of the Galaxy (e.g. globular clusters, Bulge). The Blazhko effect was found to be multi-periodic in many cases. As the same was found for the *Kepler* RRab stars, i.e. the Blazhko effect behaves in the same way for RRc stars.

(ii) Investigating the stars in the continuous viewing zone around the ecliptic poles the larger sample of *TESS* confirmed *Kepler*'s discovery that the so-called 'phase jump', reported in several RRc stars is nothing more than a annual-scale continuous phase change and not a sudden jump. The physical origin of this type of phase change is unknown.

(iii) For many stars, the main frequency shows quasi-periodic phase fluctuations. This fluctuation is clearly related to the additional frequencies present in the star. It is the strongest when two additional modes are excited in parallel on the star. The summation of this fluctuation over time may explain the strong, quasi-periodic or irregular O−C variations published in many non-Blazhko RRc stars.

Previous space observations, and later ground-based surveys, have identified several low-amplitude additional frequencies in the Fourier spectra of RRc stars. In our sample, we found all of these.

(iv) The incidence rate of stars with additional frequencies was found to be 82.8 per cent. Stars that do not show additional frequencies are more common among shorter-period RRc stars, while they are rare among longer-period stars. This is true for the frequencies associated with the $\ell = 8$ and $\ell = 9$ non-radial modes, but also for the f_{68} frequency of unknown origin. For the $\ell = 8$ and $\ell = 9$ non-radial modes, this behaviour is consistent with theoretical calculations. The situation is less clear for our finding that stars with shorter periods and larger amplitudes typically contain only $\ell = 9$ mode frequencies, while stars with longer periods and smaller amplitudes typically show both $\ell = 8$ and $\ell = 9$ mode frequencies.

(v) We have identified a new group of additional frequency with a period ratio of 0.602. We show that these frequencies, in at least the case of stars with shorter periods, can be explained by the appearance of $\ell = 10$ non-radial modes.

(vi) The amplitude distribution of the additional frequencies is approximately exponential, but there are significantly fewer stars with the smallest amplitudes and significantly more with the largest amplitudes than would be expected from an exponential distribution. The galactic distribution of stars with and without additional frequencies was found to be identical.

(vii) Our work confirms that the amplitude and phase of the f_{61}, f_{63} frequencies vary in time, as shown in previous publications. No clear relationship was found between the period of these variations and the main periods. The time dependence of the different frequencies appearing on the same star seems to be different. The variations of the f_{68} frequencies are at least an order of magnitude smaller than those of the f_{61} frequencies.

ACKNOWLEDGEMENTS

This paper includes data collected by the *TESS* mission. Funding for the *TESS* mission is provided by the NASA Science Mission Directorate. This research has made use of the SIMBAD database, operated at CDS, Strasbourg, France, and NASA's Astrophysics Data System (ADS). The research was partially supported by the LP2018-7 Lendület grant of the Hungarian Academy of Sciences, the 'SeismoLab' KKP-137523 Élvonal and NN-129075 grants of the Hungarian Research, Development and Innovation Office (NKFIH).

DATA AVAILABILITY

The full version of the data tables can be found in the electronic supplement as tab-1.txt, tab-2.txt, tab-3.txt and tab-6.txt. The raw FFI images taken by *TESS* satellite were accessed from Mikulski Archive for Space Telescopes (https://mast.stsci.edu/portal/Mashup/Clients/Mast/Portal.html) while the light

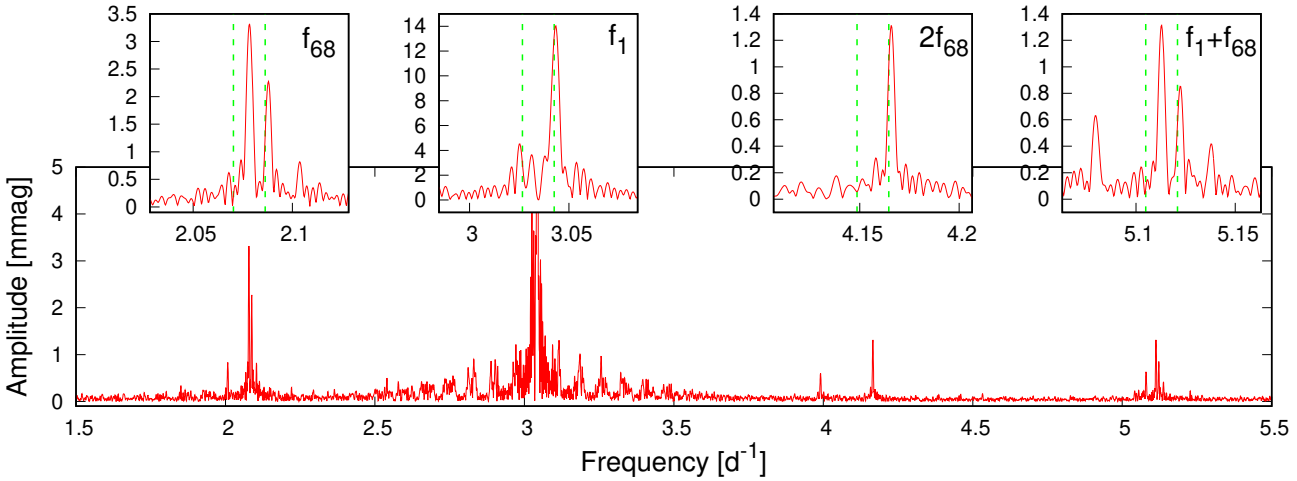

Figure 19. Extract of the pre-whitened spectrum of the Blazhko star V420 Dra. In the zoomed parts, it can be clearly seen that the Blazhko effect is also affecting the f_{68} frequency. The dashed vertical lines show the positions of the first-order Blazhko side peaks.

curves underlying this article are available via our web site (https://www.konkoly.hu/KIK/). All other data generated in this research will be shared on reasonable request to the corresponding author.

REFERENCES

Balázs-Detre J., Detre L., 1965, Veroeffentlichungen der Remeis-Sternwarte zu Bamberg, 27, 184
Balona L. A., et al., 2013, MNRAS, 432, 2808
Bellinger E. P., Kanbur S. M., Bhardwaj A., Marconi M., 2020, MNRAS, 491, 4752
Benkő J. M., et al., 2010, MNRAS, 409, 1585
Benkő J. M., Szabó R., Paparó M., 2011, MNRAS, 417, 974
Benkő J. M., Plachy E., Szabó R., Molnár L., Kolláth Z., 2014, ApJS, 213, 31
Benkő J. M., Szabó R., Derekas A., Sódor Á., 2016, MNRAS, 463, 1769
Benkő J. M., Jurcsik J., Derekas A., 2019, MNRAS, 485, 5897
Benkő J. M., Sódor Á., Pál A., 2021, Acta Astron., 71, 55
Berdnikov L. N., Dagne T., Kniazev A. Y., Dambis A. K., 2017, Information Bulletin on Variable Stars, 6212, 1
Bódi A., Szabó P., Plachy E., Molnár L., Szabó R., 2022, PASP, 134, 014503
Chadid M., 2012, A&A, 540, A68
Chadid M., et al., 2010, A&A, 510, A39
Clementini G., et al., 2019, A&A, 622, A60
Cox J. P., 1980, Theory of Stellar Pulsation. Princeton Series in Astrophysics Vol. 2, Princeton University Press
Derekas A., Kiss L. L., Udalski A., Bedding T. R., Szatmáry K., 2004, MNRAS, 354, 821
Derekas A., et al., 2012, MNRAS, 425, 1312
Dziembowski W., 1977, Acta Astron., 27, 95
Dziembowski W. A., 2016, Communications of the Konkoly Observatory Hungary, 105, 23
Forró A., Szabó R., Bódi A., Császár K., 2022, ApJS, 260, 20
Gaia Collaboration et al., 2018, A&A, 616, A1
Gruberbauer M., et al., 2007, MNRAS, 379, 1498
Johnson N. L., Kemp A. W., Kotz S., 2005, Univariate Discrete Distributions. John Wiley & Sons, Inc., doi:10.1002/0471715816
Jurcsik J., Clement C., Geyer E. H., Domsa I., 2001, AJ, 121, 951
Jurcsik J., et al., 2012, MNRAS, 419, 2173
Jurcsik J., et al., 2015, ApJS, 219, 25
Kallinger T., Reegen P., Weiss W. W., 2008, A&A, 481, 571
Karczmarek P., Wiktorowicz G., Iłkiewicz K., Smolec R., Stępień K., Pietrzyński G., Gieren W., Belczynski K., 2017, MNRAS, 466, 2842
Kovács G., 2018, A&A, 614, L4
Kurtz D. W., Shibahashi H., Murphy S. J., Bedding T. R., Bowman D. M., 2015, MNRAS, 450, 3015
Kurtz D. W., Bowman D. M., Ebo S. J., Moskalik P., Handberg R., Lund M. N., 2016, MNRAS, 455, 1237
Le Borgne J. F., et al., 2007, A&A, 476, 307
Li L. J., Qian S. B., 2014, MNRAS, 444, 600
Li L. J., Qian S. B., Zhu L. Y., 2022, MNRAS, 510, 6050
Lombard F., Koen C., 1993, MNRAS, 263, 309
Lund M. N., et al., 2021, ApJS, 257, 53
Marconi M., et al., 2015, ApJ, 808, 50
Molnár L., et al., 2015, MNRAS, 452, 4283
Molnár L., et al., 2022, ApJS, 258, 8
Moskalik P., 2013, in Suárez J. C., Garrido R., Balona L. A., Christensen-Dalsgaard J., eds, Astrophysics and Space Science Proceedings Vol. 31, Stellar Pulsations: Impact of New Instrumentation and New Insights. p. 103 (arXiv:1208.4246), doi:10.1007/978-3-642-29630-7_21
Moskalik P., Kołaczkowski Z., 2009, MNRAS, 394, 1649
Moskalik P., et al., 2015, MNRAS, 447, 2348
Netzel H., Kolenberg K., 2021, MNRAS, 508, 3508
Netzel H., Smolec R., 2019, MNRAS, 487, 5584
Netzel H., Smolec R., 2022, MNRAS, 515, 3439
Netzel H., Smolec R., Dziembowski W., 2015a, MNRAS, 451, L25
Netzel H., Smolec R., Moskalik P., 2015b, MNRAS, 453, 2022
Netzel H., Smolec R., Soszyński I., Udalski A., 2018, MNRAS, 480, 1229
Odell A. P., Sreedhar Y. H., 2016, Information Bulletin on Variable Stars, 6180, 1
Olech A., Moskalik P., 2009, A&A, 494, L17
Pál A., 2012, MNRAS, 421, 1825
Percy J. R., Tan P. J., 2013, JAAVSO, 41, 75
Pietrzyński G., et al., 2012, Nature, 484, 75
Plachy E., et al., 2019, ApJS, 244, 32
Plachy E., et al., 2021, ApJS, 253, 11
Press W. H., Teukolsky S. A., 1988, Computers in Physics, 2, 74
Prudil Z., Smolec R., Skarka M., Netzel H., 2017, MNRAS, 465, 4074
Reegen P., 2007, A&A, 467, 1353
Reegen P., 2011, Communications in Asteroseismology, 163, 99
Ricker G. R., et al., 2015, Journal of Astronomical Telescopes, Instruments, and Systems, 1, 014003
Simon N. R., Lee A. S., 1981, ApJ, 248, 291
Smolec R., Moskalik P., Kałużny J., Pych W., Różyczka M., Thompson I. B., 2017, MNRAS, 467, 2349
Sódor Á., Skarka M., Liška J., Bognár Z., 2017, MNRAS, 465, L1
Soszyński I., et al., 2008, Acta Astron., 58, 163
Soszyński I., et al., 2010, Acta Astron., 60, 17
Soszyński I., et al., 2014, Acta Astron., 64, 177

Soszyński I., et al., 2016a, Acta Astron., 66, 131
Soszyński I., et al., 2016b, MNRAS, 463, 1332
Soszyński I., et al., 2019, Acta Astron., 69, 321
Stassun K. G., et al., 2019, AJ, 158, 138
Sterken C., 2005, in Sterken C., ed., Astronomical Society of the Pacific Conference Series Vol. 335, The Light-Time Effect in Astrophysics: Causes and cures of the O-C diagram. p. 3
Sterne T. E., 1934, Harvard College Observatory Circular, 386, 30
Süveges M., Anderson R. I., 2018, MNRAS, 478, 1425
Szabó R., et al., 2014, A&A, 570, A100
Szeidl B., Hurta Z., Jurcsik J., Clement C., Lovas M., 2011, MNRAS, 411, 1744
Virtanen P., et al., 2020, Nature Methods, 17, 261
Wils P., 2008, Peremennye Zvezdy, 28, 1
Wils P., Otero S. A., Hambsch F. J., 2007, Information Bulletin on Variable Stars, 5765, 1
Wolfram Research, Inc. 2021, Mathematica, Version 12.3.1, https://www.wolfram.com/mathematica

This paper has been typeset from a TEX/LATEX file prepared by the author.